TAMPEREEN TEKNILLINEN YLIOPISTO
TAMPERE UNIVERSITY OF TECHNOLOGY

QIU FANG

CHANNEL SIMULATORS FOR MMWAVE AND 5G APPLICATIONS

Master of Science Thesis

Examiner: Associate Prof. E. S. Lohan
Examiner and topic approved on 7th Dec. 2016

ABSTRACT

QIU FANG: Channel simulators for mmWave and 5G applications
Tampere University of technology
Master of Science Thesis, 52 pages, 0 Appendix pages
May 2017
Master's Degree Programme in Information Technology
Major: Wireless Communication
Examiner: Associate Professor E.S.Lohan

Keywords: 5G, wireless communication, millimeter-wave, WINNER, QuaDRiGa, channel model, simulation

Along with the tremendous growth of extremely high traffic demand, 5G radio access technology, is becoming the core component to support massive and multifarious connected devices and real-time, and to offer high reliability wireless communications with high data rate. However, in order to enable the specification of 5G technologies, millimeter-wave (mmWave) range with a huge frequency spectrum from 3 GHz to 300GHz will perfectly meet the multi-gigabit communicative demand. However, mmWave usage also generally brings new challenges, such as coping with high attenuation or path losses.

As an effective method to evaluate the performance of the new concept in communication networks, nowadays, several channel models and simulators have been proposed and developped, such as, WINNER, COST-2100, IMT-Advanced, METIS, NYU Wireless and QuaDRiGa etc. Some of them, such as WINNER and QuaDRiGa, which is an extension of WINNER channel models, provide freely open source data, while others, such as METIS channels, are under proprietary licences. The thesis goals have been to offer an overview of the advantages and disadvantages of various mmWave channel models existing in the literature, based on the published literature, and to compare based on simulations some of the main features of two selected open-source models, namely the WINNER 2 and QuaDRiGa channel models. The propagation paths through WNNER 2 and QuaDRiGa channel modes are relying on both the line-of-sight (LOS) and non-line of sigh (NLOS) propagation models. The channel capacity criterion, investigated in our simulations with on the Binary Phase Shift Keying (BPSK) waveforms, shows that in WINNER 2, the LOS signals are received with stronger power comparing with QuaDRiGa. In the future, more mmWave channel models are planned to be tested and simulated for a better understanding of their suitability for various mmWave applications.

PREFACE

This thesis is written in partial fulfilment of the requirement for the Master of Science degree in Electrical Engineering, at the Department of Electronics and Communications Engineering, Tampere University of Technology, Finland. All the research covered under this work are done at TUT and Unicom Labs, under the supervision of Associate Professor E.S.Lohan.

I would like to give my sincere thanks to my esteemed supervisor, E.S.Lohan, who always guides me a right way through the whole work. Her professionalism and passion encouraged me to knock the door of the work successfully. I would also express my gratitude to my group-mates, classmates and friends in TUT, we shared all the precious working and studying memories together.

My appreciate goes to my father Xing Fang, mother Mingying Song, uncle Chun Fang and grandparents whose constant support and encouragement have been considered as the most cogent motivation for me. Specially, I also want to take this opportunity to thank my fiancée, Hanlu Yan. Each sprint in life are accompanied by you.

I dedicate this thesis to them all.

Thank you!

Beijing, 20.5.2017

Qiu Fang

CONTENTS

LIST OF FIGURES

LIST OF TABLES

LIST OF ABBREVIATIONS AND SYMBOLS

3GPP	3rd Generation Partnership Project
BPSK	Binary Phase Shift Keying
BS-MRS	Base Station-Mobile Relay Station
CCFD	Co-frequency Co-time Full Duplex
CDMA	Code Division Multiple Access
CP	Cyclic Prefix
CSI	Channel Station Information
CUE	Cellular User Equipment
D2D	Device-to-Device
DFT-OFDM	Discrete Fourier Transform-Orthogonal Frequency Division Multiplexing
DL	Downlink
DPC	Dirty Paper Coding
EHF	Extremely High Frequency
eMTC	Enhanced Machine Type Communication
FBMA	Filter Bank Multiple Carrier
FDD	Frequency Division Duplex
GFDM	Generalized Frequency Division Multiplexing
HetNet	Heterogeneous Network
ICI	Inter Carrier Interference
IoT	Internet of Thing
ISI	Inter Symbol Interference
LMDS	Local Multipoint Distribution Service
LoRa	Long Range
LOS	Line of Sigh
LPN	Low Power Node
LTE	Long Term Evolution
Massive MIMO	Massive Multi-input Multi-output
METIS	Mobile and Wireless Communications Enablers for Twenty-tweny Information Society
MiWEBA	Millimeter-Wave Evolution for Backhaul and Access
MMSE	Minimum Mean Square Error
MMWave	Millimeter-Wave
MRT	Max Ratio Transmit
NB-IoT	Narrowband-Internet of thing
NLOS	Non-Line of Sight
NOMA	Non-orthogonal Multiple Access
OFDM	Orthogonal Frequency Division Multiplexing
OFDMA	Orthogonal Frequency Division Multiple Access
OMA	Orthogonal Multiple Access
PCB	Printed Circuit Board
QPSK	Quadri Phase Shift Key
QuaDRiGa	QUAsi Deterministic Radio Channel Generator
RF	Radio Frequency
SCM	Spatial Channel Model
SHF	Super High Frequency
SNR	Signal to Noise Ratio
TDD	Time Division Duplex

UDN	Ultra-Dense Network
UE	User Equipment
UFMC	Universal Filter Multiple Carrier
UHF	Ultra High Freqency
UL	Uplink
VFH	Very High Frequency
WINNER	Wireless World Initiative for New Radio
WLAN	Wireless Local Area Network
WPAN	Wireless Personal Area Network
ZF	Zero Force

Δf_D	change of frequency
$\mathbf{B}_{\mathrm{D}}$	Doppler spectrum width
$\mathbf{H}_{\mathrm{n}}$	channel matrix
$\mathbf{L}_{sh}$	shadow loss
$\boldsymbol{F}_{tx}$	transmitter antenna array matrix
σ_{Φ}	angle spread
c	the speed of light
D	distribution density
G	antenna gain
g	antenna pattern
i	node
I	path segment
k	pathway
P	power
R	distance
s	transmitter antenna element
u	receiver antenna element
v	Doppler frequency component
β	ratio power of reflection
Δs	tile area
λ	wavelength
τ	delay
r	location vector
Φ	angle of departure
φ	angle of arrival
ψ	pahse
ω	ramp range

.

1. INTRODUCTION

Along with the tremendous growth of extremely high traffic demand, 5G radio access technology is becoming a key component of the information society [1]. The overall objective for 5G is to support massive and multifarious connected devices and satisfy the real-time, high reliability communications. However, in order to enable the specification of 5G technologies, many challenges still remains such as, designing new flexible air interface, achieving a large system capacity, and addressing the possible spectrum shortage etc.

1.1 Millimeter-wave application

With huge bandwidth, 3-300 GHz spectra are collectively referred to as mmWave bands. For the demand of high bandwidth connectivity, mmWave communications are proposed to be one of the enablers for 5G networks providing multi-gigabit communicative applications, such as high definition television (HDTV) and ultra-high definition video (UHDV) [2, 3]. In general, one of the most important features of mmWave is the high attenuation and penetration in free space, which enable the same frequency to be efficiently reused at short distance. The mmWave frequencies with large spectrum resource can be used for various services, including the local multiple point services from 28 GHz to 30 GHz, the free licensed band at 60 GHz, and the E band containing 71-76 GHz, 81-86 GHz, and 92-95 GHz [4] and promoting several standards definition for indoor wireless personal area networks (WPANs) and, wireless local area networks (WLANs), such as ECMA-387 [5,6], IEEE 802.15.3c [7], and IEEE 802.11ad [8]. Both the cellular systems and outdoor mesh networks are greatly becoming attractive in mmWave band [9-13].In 60 GHz mmWave, typically directional antennas are applied in order to compensate the large path loss and penetration attenuation in non-line of sight (NLOS) environment. Compared with lower frequencies spectrum, the directional transmission link formed between directional antennas at transmitter and receiver is activated with larger gain and less interference to each other at mmWave. However, the antenna beamwidth on mmWave band is narrower than that on the lower bands, which practically brings in a significant challenge to conduct axis alignment and aligned axes based positioning [14]. Correlatively, the mmWave with high frequency accounts for implementing small physical size of antennas, especially for building complex antenna arrays and integrating them on PCBs (printed circuit board). Moreover, transmission on the extremely high frequency band has a limited range, together with the narrow beamwidth, rain attenuation, and atmospheric absorption, the mmWave provides is privacy and security.

1.2 Existing simulators and channel models

As an effective method to evaluate the performance of new concepts in communication networks, channel modes and simulations are proposed and verified frequently and innovatively. MmWave, regarding as the core frequency candidate for 5G, is able to offering dramatically high data rate in broadband mobile and backhaul services [15], [16]. Hence, suitable channel models and accurate parameters for mmWave communication are urgent for implementation of the link and system level simulations particularly. Recently, the indoor radio channels characteristics in frequency bands, such as 10 GHz, 11 GHz [17-19], 60 GHz [20, 21], and 70-73 GHz [22] have been studied, as well as the campaigns for outdoor urban cellular networks have been performed in 10 GHz, 18 GHz, 28 GHz, 32 GHz, 38GHz, 60 GHz, 72 GHz, and 81-86 GHz [27,28].

Unlike in lower bands, the extremely high frequencies' performance is prominent, which leads to particular features of transmission propagation channel suffering high diffraction loss, high diffusion and sensitivity to attenuations in specific environment, such as rain and foliage. Accordingly, the previous channel models designed for sub-6 GHz are particularly not useful, as they are not able to model various effects occurring at mmWave carrier frequencies. The adaptable models have to be designed in such a way to achieve both accuracy and implementation efficiency in air interface and system performance for mmWave communications [15, 29].

Based on the extensive research of the mmWave channel [29-34], several models have been built. For example, a map-based ray tracing model of METIS [30], the geometry based quasi-deterministic model of Millimetre-Wave Evolution for Backhaul and Access (MiWEBA) [31] and a statistical models based on power-delay-angular distributions [32, 33]. In METIS, the detailed map of Manhattan and Madrid are applied to measure the electromagnetic energy interactions. Continuously, more projects corresponding to 5G mmWave channel modeling works have been conducted, including NYU Wireless [22, 23], 3GPP [35], QuaDRiGa [35], and so on.

In this thesis, we primarily introduce the 5G technology with the particular features and advantages, then we summarize the physical layer characteristics for 5G proposed signals and technologies, such as Massive multi-input multi-output (Massive MIMO), non-orthogonal multiple access (NOMA), Co-frequency Co-time Full Duplex (CCFD), device-to-device (D2D), ultra-dense network (UDN) and the modulation schemes. Together with the analysis about the mmWave application, the research has been conducted based on recently existing 5G and mmWave channel models and the simulations. Furthermore, we compared two channel models with simulations, namely WINNER 2 and its extension one QuDRiGa, and we make a comparative table among most of popular channel models.

1.3 Author's contributions

The contributions to this thesis of the author can be summarized as follow

1) an extensive Internet search of various mmWave existing channel simulator
2) a literature overview of 5G channel models and 5G main characteristics
3) a basic investigation of the suitability of the found open source mmWave simulator for communications and positioning studies
4) an elementary simulation-based comparison of two selected mmWave simlators
5) a theoretical comparison of various mmWave simulators with their advantages and disadvantages

1.4 Thesis structure

The thesis is structured as follows. Chapter 1 gives a brief overview of the motivation and goals of the thesis and the author's contribution. Chapter 2 presents a general view of 5G technologies, such as the physical layer and a brief introduction about Internet of Things (IoT). Chapter 3 focuses on mmWave communication, together with applications and challenges. Chapter 4 deals with the mostly popular channel models, such as WINNER 2, METIS, and QuaDRiGa and illustrates a comprehensive comparison among them. Chapter 5 implements some simulations based on WINNER 2 and QuaDRiGa channel models and analyses their main features. Finally, chapter 6 presents the conclusions.

2. 5G AND THE INTERNET OF THINGS

5G, as a new wireless mobile communication network, is developed for fulfilling the demand of mobile communications in 2020 and beyond. A relevant vision of 5G says that it is a blend of pre-existing technologies, covering 2G, 3G, 4G, WiFi and others, in order to allow higher coverage and availability, and higher network density in terms of cells and devices, with the greater connectivity for machine-to-machine services and the Internet of Things [128]. As being considered to be faster than existing technologies, 5G, with a promising prospect, enhances the applications with high social and economic value. Although 5G systems is still under experimental phase with inedited not-yet-available technical standard, it is becoming the hot issue among worldwide research institutes of mobile communications, such as METIS [104], IMT-2020 [129], 5G-PPP [130], etc. The ultimate goal for 5G is to realize seamless connection and reliable global communication. Because of the rapid development of Internet and ever-increasing requirement of IoT, 5G is promoted to have low cost and energy consumption, to be secure and reliable, to offer 10 to 100 times of simultaneous transmission rate than 4G systems, to reach 10 Gbit/s of peak transmission rate, to have 10-100 times of density of devices connection and 5-10 times of spectrum efficiency compared to 4G systems, etc. In a word, 5G is the future, which breaks the obstacle of time and space, where access of sharing data can be anywhere, anytime to anyone with anything [37]. Basically, four main features of 5G are listed as below:

- Efficient frequency spectrum resources
  Frequency bands from 300 MHz to 3 GHz are under intensive occupation nowadays [38], and this limitation of spectrum source has led researchers to exploit new bands, mainly from 3GHz to 300 GHz, for developing 5G and 5G+ generations [39]. In the meantime, Very High Frequency (VFH) and Ultra High Frequency (UHF) are commonly used in the already existed communication systems. Specifically, VFH, from 30 MHz to 300 MHz with corresponding wavelength from 10 m to1 m, is attenuated quickly and it is primarily adopted to short distance transmission in space wave form. Thereby, VFH is highly influenced by the troposphere, and greatly depending on the terrain and ground feature. Nevertheless, it can be used in the aviation industry and ensure the unblocked communication among airplanes and between air segment and ground segment during the flight. Moreover, Ultra High Frequency (UHF) ranges from 300 MHz to 3000 MHz, with wavelength from 100 cm to 10 cm. The decimeter wave is also suitable for short range communication with advantages of good penetrability. Thus, UHF is effectively applied in mobile and wireless communication, and is broadcasting in the form of ground space wave.

- **High system capacity**
  The information society will step into a big data era with the boost of mobile internet. Consequently, it is expected that the communication traffic, user data rate, number of connection devices will increase drastically. Thus, 5G mobile communication systems are designed to be available to support the high system capacity requirements.
- **Better user experience**
  User experience with efficient, secure, steady wireless internet environment will be the key factors, especially after data rate reaching a satisfying value to cope with majority mobile data services and applications.
- **Low power consumption**
  Under the premise of fulfilling the service of requirement, the quality of service and the user experience, wireless communications in the future aims to be green and eco-friendly communications.

Specifically, a set of eight requirements have been identified by vendors and organizations, such as Ericsson [40], Huawei [41], 5G-PPP [42], etc.

- Up to 10Gbps data rate, which means 10 to 100 times of improvement over 4G and 4.5G networks
- 1 millisecond latency
- 1000 times large of bandwidth per unit area
- Up to 100 times of number of connected devices per unit area (compared with 4G LTE)
- 99.999% availability of service
- 100% coverage
- 90% reduction in network energy usage
- Up to 10-year battery life for low power IoT devices

2.1 5G characteristics and features

The development and deployment of 5G are dependent on the existing and emerging key technologies. In this section, several 5G physical layer key techniques are introduced, namely massive MIMO, NOMA, full duplex for doubling spectral efficiency, D2D, mmWave communications, wideband communications and dense network of access nodes, etc.

2.1.1 Massive MIMO

Traditionally, MIMO has been studied extensively in 3G and 4G systems and applied to mobile communication systems, such as 3G, LTE, WiFi etc. In the year of 2010, Marzetta

proposed an original idea by deploying large scale of antennas instead of the multi-antenna [43]. Then, in order to meet with the demand of high speed data traffic, it evolved into the massive MIMO wireless communication theory. Massive MIMO concept has incomparable advantages in improving spectrum efficiency, increasing quality of transmission signals and enhancing the system coverage area, etc. As indicated in [43], "*by increasing the number of antennas at the base station, we can average out the effects of fading, thermal noise and intra-cell interference*". And in the application of both law of large numbers and central limit theorem, the design of Massive MIMO system is no longer needed to be nonlinear, and signal processing methods can be realized in linear way to avoid the above mentioned interferences and improve the system performance. For example, in the aspect of precoding the traditional MIMO system is normally focused on nonlinear precoding, such as dirty paper coding (DPC), while Massive MIMO systems are implemented with linear precoding: max ratio transmit (MRT), zero force (ZF) and minimum mean square error (MMSE). And according to [44], the experiment reported in there illustrated that by applying linear precoding methods with lower computing complexity, the system can achieve 98% of performance of what DPC has done. In other words, the simplest linear precoding and decoding algorithm converge to an optimization as well [43].

The research of massive MIMO technology is an emerging field even with gratifying progress, but still some problems are left to be solved. With the growth of antenna amount, the accurate channel state information (CSI) is requested in a transmitter or base station in order BS to ensure the reliability [45]. To acquire the expected CSI, time division duplex (TDD) system is an efficient method, which uses the reciprocity of channel state at both uplink and downlink in relevant time, moreover, in the same frequency [46-48]. In frequency division duplex (FDD), the uplink (UP) and downlink (DL) use different frequencies, which means that the CSI referring to the uplink and downlink is not the same. The term of the uplink channel estimation is done at the base station while all different pilot sequences from users are sent to. And the required time for uplink transmitting pilots is independent from the antennas at the base station. Continuously, two steps are needed to get CSI for the downlink channel. Pilot symbols will be transmitted to all users by the base station, then users send estimated CSI to the base station with feedback. However, the time for transmission to the base station is proportional with the number of antennas. As the number of antennas at base station increases, the FDD system becomes impracticable. Comparatively, only CSI for the uplink is required to be estimated in TDD. And in a concise way, a base station receives the users' pilot sequences and uses the estimated CSI to detect the uplink data, and it also can support for downlink data transmission. However, [49] indicates another problem causes by applying TDD that is named pilot contamination. Briefly, the pilot sequences generated by users in adjacent cells are no longer staying orthogonal, since the coherence time is limited.

2.1.2 NOMA

Technically, Orthogonal Multiple Access (OFDMA) scheme is applied in 4G for low cost and performance with a good throughput. However, for 5G, in order to achieve approximately 5 to 15 times more spectrum efficiency than in 4G, new multiple access multiplexing methods are needed to be adopted. In Orthogonal Multiple Access (OMA) technology, every single user is allocated with source separately, while in Non-Orthogonal Multiple Access (NOMA), as shown in the Figure 2.1, the allocation is ongoing with multiuser simultaneously. Unlike a typical orthogonal transmission, a non-orthogonal transmission and successive interference cancellation are used in transmitter and receiver respectively, while carrying interference information in propagation proactively. Hereby, the aspect of receiver in NOMA is becoming more complex, but gaining higher spectral efficiency. Specifically, the key features of NOMA are that allocating multiuser at different power levels and successive interference cancellation.

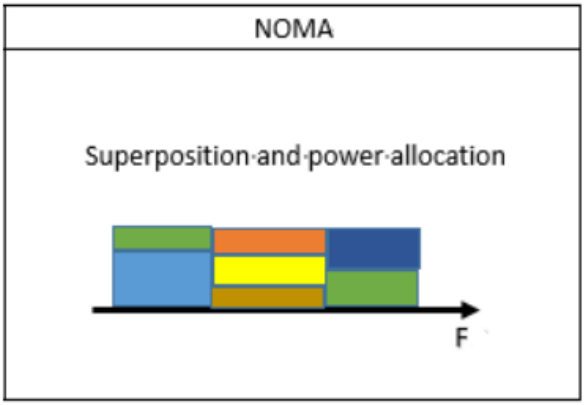

(a)

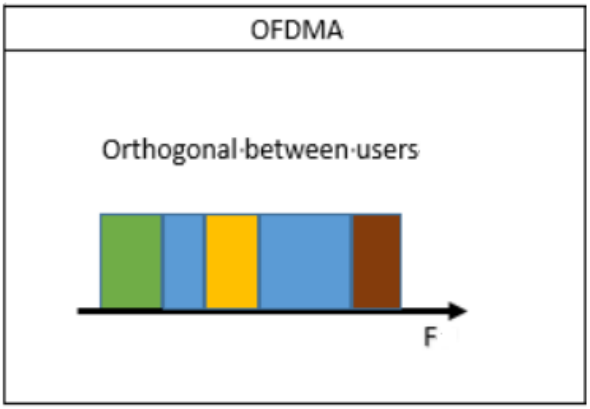

(b)

Figure 2.1 *Illustration of* ***(a)*** *OFDMA and* ***(b)*** *NOMA principles*

Due to the fact that the dramatic growth of multimedia services cannot match the rare radio frequency resources, NOMA is developing to improve the spectral efficiency in

the design of future wireless communication systems and becoming a key enabler for implementation of 5G.

2.1.3 Full duplex

In 4G systems, FDD and time division duplex (TDD) are working with two separate channels to generate orthogonal transmission and reception. However, full duplex can promote the spectrum efficiency by transceiving simultaneously on both the same frequency and time. Due to the efficiency characteristic, full duplex is also widely accepted as one of the promising techniques in 5G network. Co-frequency Co-time Full Duplex (CCFD) was proposed by G. R. Kenworthy in his paper in 1997 [50]. In CCFD wireless communication, signals are transmitted and received simultaneously in the same frequency, thus, the spectral efficiency in radio link is increased by double. As showing in Figure 2.2, the far-end and near-end units are transmitting in the same time and frequency bandwidth. Comparing with existing TDD and FDD systems, the frequency efficiency can be promoted over one time theoretically.

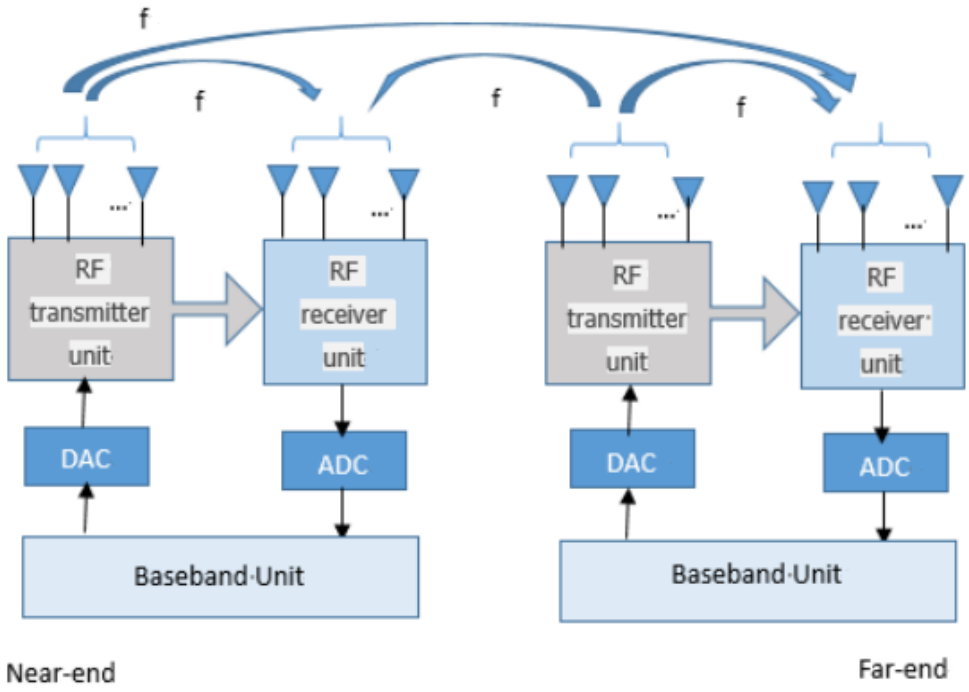

***Figure 2.2** CCFD diagram*

However, due to the co-frequency and co-time transceiving, the signal propagated by the transmitter may generate interference to the local receiver. As we know, the radio signals attenuate through propagation. Moreover signals from local station always have much stronger power than that from other base stations (near far effect). In this case, the main problem is self-interference cancellation and suppression, which directly affects the communication quality of systems. In [50], the authors describe two methods to eliminate

self-interference, which are radio frequency cancellation and digital interference cancellation technologies. Also a new method called antenna cancellation was proposed in [51]. Briefly, is that it installs two antennas at transmitter and a receiver antenna with reasonable distance to overcome self-interference.

2.1.4 Device-To-Device (D2D) communications

Network capacity, spectrum efficiency and terminal user experience guide the direction for 5G evolution in the future. Theoretically, D2D communication leads to the prospect of improving system's performance, enhancing user experience, and releasing load in BS. D2D communication is based on a cellular system and it is suitable for short range communication. The cellular network, consisting of User Equipment (UE) and Cellular User Equipment (CUE), acts as an underlay network where channel resources can be shared from D2D pairs to existing cellular UEs and CUEs. In D2D, data are transmitted among terminal devices without transferring at BS and relevant control signals. Under the condition of employing D2D communication in cellular network, the scheme of direct transmission relieves the BS load and reduces transmission delay, lowers the terminal transmitting power and furthermore, it raises spectrum efficiency [52]. For special cases, such as partially damaged wireless communication infrastructures and blind zone, where there is no Long Term Evolution (LTE) networks, terminals through D2D are still eligible for communication and even get access to the cellular.

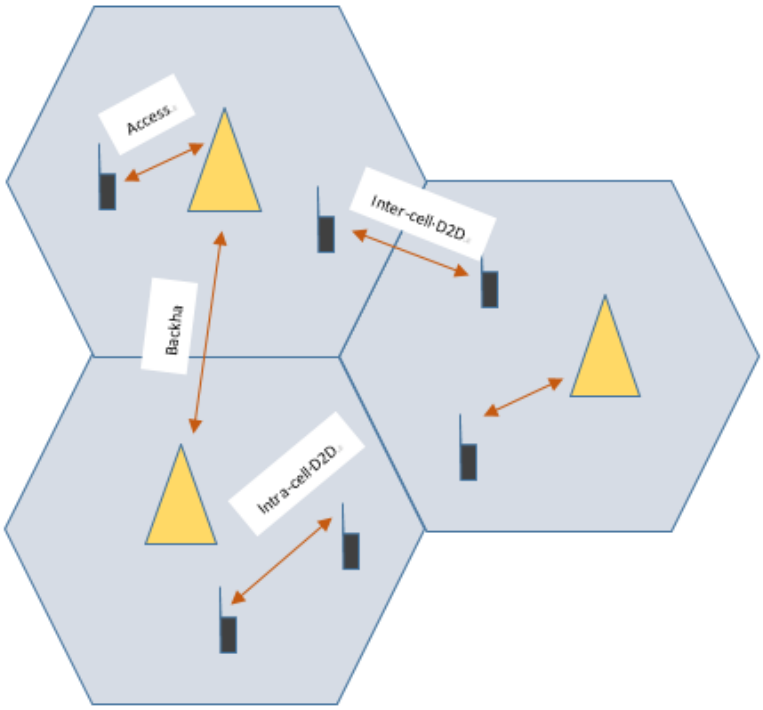

Figure 2.3 *D2D system diagram*

Figure 2.3 shows the D2D system diagram, which illustrates that communication among users happens both intra-cells and inter-cells through D2D links. In the immediate future

with the explosive growth of terminal number, the access of D2D network is proposed to relieve the challenge of access load for BS. However, in a non-orthogonal co-channel networks, as in Figure 2.3, the interference from base station to D2D transmission line is definitely covering the resource share from any D2D pairs. Continuously, when D2D pairs share uplink cellular resources standing closed to a CUE, the desired CUE uplink transmission will be ruined. And the same happens for the co-channel pairs if it is surrounded by any other strong interference. In [53], the authors apply mmWave transmission into the D2D systems, Thus, D2D communications may change into orthogonal dedicated channel model with massive available resources in mmWave bands. With the directional and narrow beam, the transmission is always eligible for relieving interference and increasing spatial gain. As illustrated in the Figure 2.4 (a), when the D2D pair 1, in the condition of downlink and located nearby the BS, is not affected by the main lobe of BS transmitting beam, it will stay active. For the uplink case of Figure 2.4 (b), the CUE 1 can complete its transmission as well as the co-channel works as normal, and the interference from D2D pair 2 can be neglected. In conclusion, the performance of D2D systems with implementation of mmWave transmission will be largely enhanced.

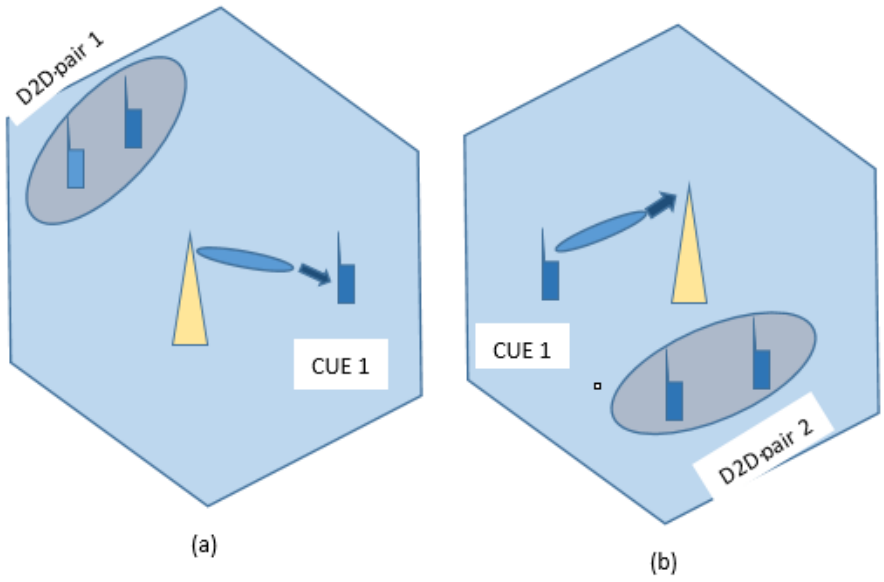

Figure 2.4 *MmWave transmission in non-orthogonal D2D communications*

2.1.5 MmWave and wideband communications

Almost all the operating frequencies in commercial wireless communication are aggregated from 300 MHz to 3 GHz. Thus, the current spectrum under 3 GHz becomes increasingly crowded. However, the utilization of frequency bands from 3 GHz to 300 GHz, known as mmWave, is still low and it is offering a chance for the reserved 5G system. Overall, the main challenges are path loss, penetration loss and rain attenuation. Basically, with the decreasing of wavelength or improving of frequency, the loss of free space propagation will increase according to the free space propagation [54] model. In addition, the

term of low frequency signal has advantages of being easier to penetrate buildings and walls, which is explained in more detail in Section 3.

As we know, the channel capacity is in directly proportion to both the available bandwidth and the Signal to Noise Ratio (SNR), and the higher frequencies provides larger channel capacity, as well as larger available bandwidth. Therefore, in order to support the data rate in 5G network, the ultrabroad-band spectrum is a logical choice. Even a simplified modulation technique, such as QPSK, can achieve 10Gpbs data rate in 1GHz wideband by combining with spectrum efficiency promotion like techniques, such as massive MIMO [55].

2.1.6 Ultra-dense Heterogeneous Networks (UDN)

5G networks are developing towards diversification, broadband, totalization and intellectualization. In the year of 2020, the mobile data traffic is forecast to have an unprecedented growth. One of the core approaches is to reduce the cell radius and to improve the low power node (LPN), which is able to result in satisfying 1000 times large of data traffic than ever before [56-58]. Thus ultra-dense Heterogeneous Network is considered to be a crucial method.

More than 10 times of number of existing wireless nodes will be installed in the future. Specifically, the sites are located near to others within 10m while supporting 25000 users with the coverage of 1 km^2 [59-61]. At the same time, the number of active users and the number of active nodes will happen to be in the ratio of 1:1, which means one-to-one correspondence [62]. A dense networking can shorten the distance between terminals and nodes, and it can also enhance the power and spectrum efficiency, meanwhile improving the network coverage and system capacity [62]. Although UDN is eligible for a promising application development prospect, the distance among nodes still causes a complicated network topology which leading to the problem of incompatibility of the HetNet with existing mobile communication systems. In 5G mobile communications, interferences, such as same frequency interference or, sharing spectrum interference [63-65], are non-negligible. Moreover, adjacent nodes with similar transmission loss lead to a recognition problem, which makes the network performance worse. To solve it, new handover algorithms [66], designed for recognizing adjacent nodes effectively [67], are urgently needed, while existing coordination algorithms can only handle single interference source.

2.2 Modulation types in 5G

In communication system, baseband signals are transformed through channel transmission only after having been modulated. Thereby, the validity and reliability of transmission are highly depended on the modulation schemes. At present, two primary mechanisms are applied. One is the single carrier spread spectrum technology, such as CDMA (code division multiple access). The second one is the multicarrier modulation technique,

such as OFDM. Briefly, OFDM (orthogonal frequency division multiplexing) is widely implemented in wireless communication, with advantages of spectral efficiency, lower complexity and good performance through multi-path propagation. In 5G system, a number of multicarrier waveforms scenarios are proposed, such as FBMC (filter bank multi carrier), UFMC (universal filter multi carrier), Discrete Fourier transform-Orthogonal Frequency Division Multiplexing (DFT-OFDM) and GFDM (generalized frequency division multiplexing), etc. These are briefly overviewed in the next sections.

2.2.1 FBMC

Compared to OFDM, filters are allocated to every single subcarrier respectively in FBMC for the purpose of eliminating inter-carrier interference (ICI), and the cyclic prefix (CP) is not necessary while FBMC is based on OQAM to ensure the orthogonality and avoid inter symbol interference(ISI) [131].

2.2.2 UFMC

UFMC waveform is a derivative of OFDM waveform combined with post-filtering by utilizing individual filter per sub-band [132].

2.2.3 GFDM

GFDM waveform is based on the time-frequency filtering of a data block, which leads to a flexible, non-orthogonal waveform [68]. In GFDM, it is necessary to implement an interference cancellation scheme and add CP to the end of each block of symbols.

2.3 Introduction to IoT cocept

Defined by ITU-T, The Internet of Things is "*a global infrastructure for the information society, enabling advanced services by interconnecting (physical and virtual) things based on existing and evolving interoperable information and communication technologies* (ICT)" [69]. IoT is seen as the world-wide network, which consists of various heterogeneous physical objects, such as devices, vehicles, buildings, mobile phones, sensors [70] and possible items embedded within electronics, software etc. The communication capabilities provide a smart environment with collecting and sharing data among "things". The term IoT is widely used nowadays and covering an extensive range of fields, including healthcare, transportation, smart city, home automation, especially wireless communication.

IoT is composed of different networks which are conducted with individual objectives. For example, combining with LPWAN (Low Power Wide Area Network) which can offers wide-area coverage in 5G technologies, is able to intend to cover wide area. It has

been addressed in the 3rd Generation Partnership Project (3GPP), also with relevant release, Rel-13. EC-GSM-IoT [71] and LTE-MTC [72]. Generally, LPWAN contains many technologies, such as LoRa, Sigfox, NB-IoT, Wireless-N, Amber Wireless, OnRamp, Telensa, eMTC and PlatanuS. These are listed below.

- **LoRa (Long Range)**
  LoRa was published in 2013 by Semtech company with a spectacular sensitivity around 111 dBm to 148 dBm, which highly illustrated the reliability of network connectivity. With the sensitivity, the communication systems can be arranged in long range, long life time of battery, large capacity and low cost. Moreover, LoRa is based on SS (spread spectrum) chirp modulation, and it is used in the unlicensed frequency bands, for example, 433 MHz, 868 MHz and 915 MHz.
- **NB-IoT**
  NB-IoT is a new 3GPP radio-access technology requiring 180 kHz minimum system bandwidth at both downlink and uplink, respectively [73]. NB-IoT follows the design of LTE extensively, utilizing OFDMA (orthogonal frequency-division multiple-access) for downlink and SC-FDMA (single-carrier frequency-division multiple-access) for uplink. The data rate is less than 100 kbps.
- **eMTC**
  LTE-M, also kown as LTE-Machine-to-Machine (M2M), is based on the evolution of IoT technologies. It is also named as Low Cost MTC and LTE enhanced MTC (eMTC) in Rel-12 and Rel-13, respectively. Its channel bandwidth is 1.4 Mbps, and peak rates are 1 Mbps at both uplink and downlink. Meanwhile, eMTC provides half-duplex FDD and TDD.

The Table 2.1 illustrates more of the LPWA technologies with reference performance.

Table 2.1 *Comparison of LPWA technologies*

	Distances (km)	Frequency	ISM-band	Symmetry of downlink and uplink	Data-rate	OTA (over-the-air technology)	Standardization
LoRa	Suburban: 15-22 Urban: 3-8	Broadband	Yes	NO	0.3-5 kbps	Yes	NO
OnRamp	4	Sub-GHz	Yes	NO	8bps-8kbps	Yes	IEEE
Platauns	Hundreds	2.4 GHz	Yes	NO	500 kbps	Yes	Weightless-p
SigFox	Rural: 50 Urban: 10	868,902	Yes	NO	100 bps	Yes	NO
Telensa	8	868,915,470	Yes	Yes	Low	Yes	NO
Amber Wireless	20	434, 868 2.4 GHz	Yes	-	500 kbps	Yes	NO

3. MMWAVE COMMUNICATION

The range of 3-30 GHz spectrum is generally known as the super high frequency (SHF) band, while 30-300 GHz is referred to as the extremely high frequency (EHF). More precisely, the frequency range from 26.5 to 300 GHz with bandwidth of 273.5 GHz is named mmWave band. In a broader definition, due to the similar propagation characteristics in both SHF and EHF, the spectrum of 3-300 GHz is sometimes collectively known as mmWave with wavelength ranging from 1 to 100 mm. In general, the EHF is transmitted in space with straight narrow beam, providing good performance of directivity and highly depended on the propagation environment, such as atmospheric absorption, obstacles, rain, etc. But due to the extremely high frequency, the mmWave communication is becoming stable and reliable with less interference sources.

With the development of 5G networking, the mmWave communication with a possible gigabit-data service, is considered as the one of the key enablers to implementation for 5G broadband cellular communication networks. The mmWave concept has been preliminarily unleashed and primarily exploited for short-range and wireless communications nowadays, as shown in the Figure 3.1.

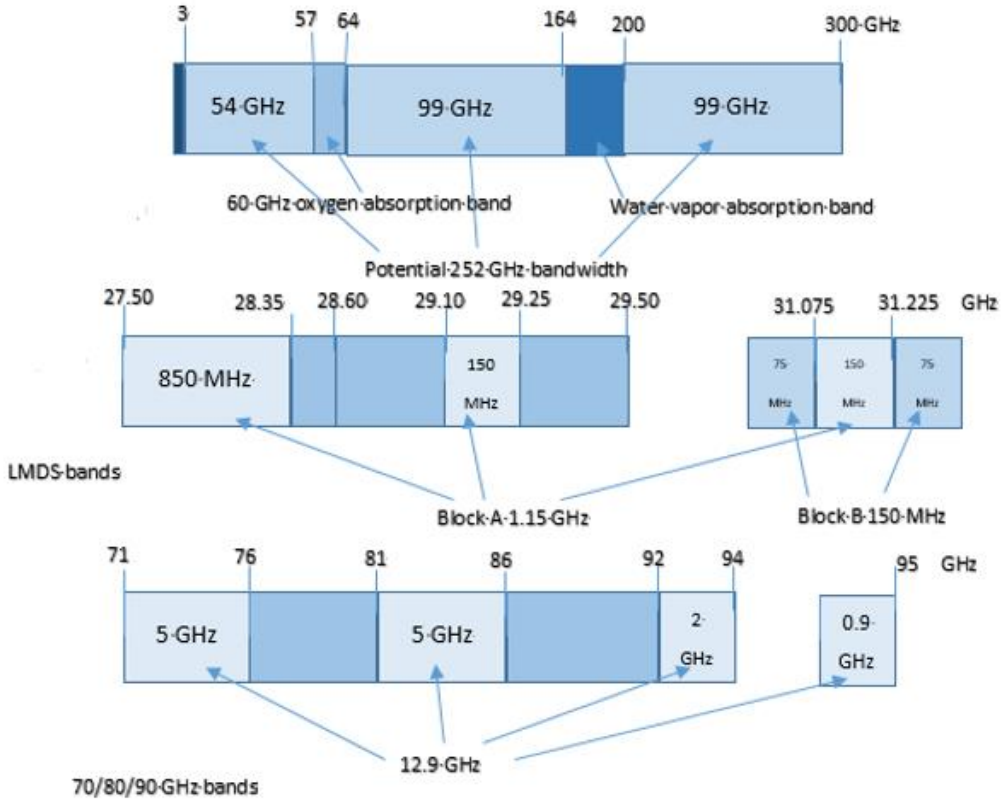

Figure 3.1 *MmWave spectrum*

The authors in [38] indicated that the unlicensed ultra-wideband (UWB) ranging from 3.1-10.6 GHz frequencies can support high data rate connectivity in personal area network. Also the band within 57-64 GHz, with oxygen absorption, is promoted to enable multiple gigabit data rates for short-range connectivity and wireless local area networks. Meanwhile, the spectrum between 164 and 200 GHz is water vapor absorption [74]. It is illustrated from the Figure. 3.1 approximately around 252 GHz bandwidth is suitable for mobile broadband. Additionally, local multipoint distribution service (LMDS), standardized by the IEEE 802 LAN/MAN Standards Committee by the IEEE 802.16.1 Task Group ("Air Interface for Fixed Broadband Wireless Access System" for 10-66 GHz) is a broadband operating on frequencies from 28 to 30 GHz. It applies a cellular infrastructure and supports point-to-multipoint communication. And later the Federal Communications Commission (FCC) auctioned two LMDS licenses of A and B block, respectively and announced three segments, 71-76 GHz, 81-86GHz and 92-95 GHz, combing as E band (71-76 GHz, 81-86 GHz, and 92-95 GHz), which is available for ultra-high-speed data communication.

3.1 Overview of the mmWave band

Since the published of mmWave communication standards for wireless personal area networks (WPAN) at 57-64 GHz and 60 GHz bands by IEEE 802.15 Task Group 3c (TG3c) [75] and IEEE 802.11ad (WiGig) [76], respectively, mmWave frequencies in future 5G cellular networks are highly stimulating for researching and potential commercial use. Additionally, an enormous amount of spectrum around 28-30 GHz carrier frequencies is investigated for the local multi-point distribution service. The free licensed band at 60 GHz and the E band, which is announced by the Federal Communications Commission (FCC) in 2003, can be dedicated for developments in 5G era. Recently, the majority of current research is focused on the 28 GHz band, the 38 GHz band, the 60 GHz band, and the E band [77]. However, there are numerous fundamental characteristics and challenges of mmWave communication should be considered when comparing with existing systems conducting in the microwaves band.

3.1.1 Beamforming technology

With small wavelength of signals in mmWave communication, a large number of transmitting antennas are implemented but with limited special radio frequency (RF) chains. And in the traditional cellular system, the number of RF chains is the same as the transmitting antenna numbers while beamforming is implemented in the baseband. As shown in Figure. 3.2, the hybrid beamforming architecture consisting of analog beamforming and digital precoding. As indicated in [16], both analog and digital beamforming in mmWave transmission are operating independently and cooperatively to optimize system

capacity through MIMO techniques. In general, the RF chain, including low noise amplifiers (LNA), down converters, A/D converters and so on, are essential at both transmitters and receivers.

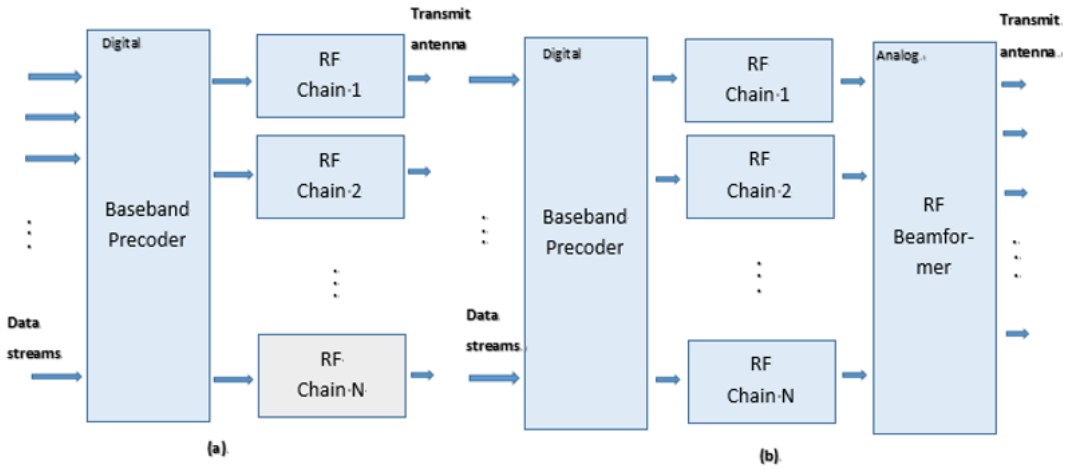

***Figure 3.2** Beamforming diagrams **(a)** sub-3 GHz **(b)** mmWave system*

Furthermore, from digital beamforming and precoding perspective, the diversity gain [78] can be reduced by using directive antennas. As an advantage, the physical size of antennas at mmWave frequencies is proposed to be small and to contain build in complex antenna arrays, in order to integrate easily into chips or PCB [79]. Afterwards, the antenna elements can be applied by altering the signal phase and steering the beam towards to make intensive gain through single direction. Besides, the directional antennas may combat fading, multi-path and interference in transmission channel, which can promote also the development of D2D [80].

3.2 Examples of mmWave applications

3.2.1 Heterogenuous Networks (HetNet)

Due to the limited coverage, it is greatly proposed to arrange mmWave communications coexisting with other systems, such as LTE and WiFi, and thus forming a heterogeneous network (HetNet). In HetNets [81], various types of base stations are co-existing, such as traditional macro ones, low power and cost micro ones, like picos, femtos, and relays in order to promote system capacity. Thereby, the cooperation and interaction among different networks in HetNet are the promising way to explore and study and solve potential problems, such as mobility, vertical handover, load balance [82], inter-cell interference, etc. As shown in Figure. 3.3, a pico-cell in 60 GHz band coexists with macro-cells and micro-cells [77]. Apparently, cells with microwave bands are performing a larger coverage and smaller cells, like BBSs (defined in IEEE 802.11ad, basic service set), in 60 GHz band are providing higher capacity. In terms of a hybrid HetNet [83], characteristics of

spectrum at 60 and 70-80 GHz are exploited to resist the interference. In [84], a combination of mmWave and 4G system is indicated. Its architecture with TDMA-based medium access control (MAC) structure is regarding as a candidate for 5G cellular network.

The mmWave communication systems with large capacity are eligible to offload traffic from the macro-cells and perform good services for traffic. Meanwhile, at both mmWave and microwave bands, the control messages are distributed for channel access and coordination [38]. In this case, control signals, such as synchronization and channel access requests, transmits in all directions in microwave and cause a tradeoff based on network coupling between complexity and performance in heterogeneous networking [77].

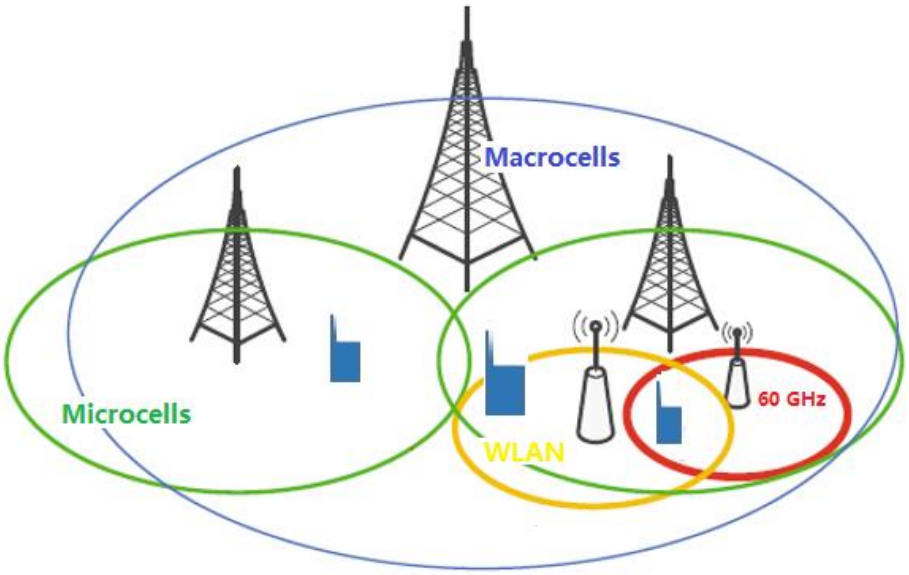

Figure 3.3 *Heterogeneous networks, including macrocells, microcells, WLANs and picocells*

3.2.2 Satellite communications

As we know, the electromagnetic waves are highly depended on their wavelength and obstacles' size while diffracting. With a small wavelength in the 60 GHz band, the transmission line is highly sensitive to blockages, for example due to humans as obstacles. However, the mmWave communications, with abundant spectrum resources and particular characteristics, can be appropriately developed for satellite communications. First, the greater penetrability through dust, smog, plasma, make mmWave satellite communications available and all-weather. Also because of the atmospheric absorption by water vapor, oxygen and rain, the straight-line distance of point-to-point communications is limited. The weak signals in the area over the distance are hard to be detected, which avoids from intercepting and interfering. The term of atmospheric window indicates frequency band at 35 GHz, 45 GHz, 94 GHz, 140 GHz and 220 GHz, at which the attenuation is reducing. In addition, mmWave can be applied in positioning application, such as emer-

gency rescue and unmanned vehicles. In [85], it says that in 5G networks traditional positioning systems like GNSS will be complemented by mmWave and massive MIMO technologies to enable the positioning services in indoors and dense urban areas where GNSS signals are not available at present.

3.3 MmWave Challenges

At present, 5G mmWave communication technologies are still in the stage of testing stage, but the mmWave band has demonstrated its potential prospects by applying it to 5G cellular systems. For example, researchers from SAMSUNG in [39] indicate that they have designed an antenna performing at 1 Gbit/s data rate at 2 km away, with beamforming in mmWave band. However, to enable mmWave communications in 5G cellular networks, there are still certain concerns referring to the extremely high frequency transmission, namely path loss, atmospheric absorption and penetrability, etc.

Traditionally, mmWave communications suffer from high transmission loss, comparing with other systems operating in lower frequencies. According to the Friis transmission law with the following equation:

$$\frac{P_r}{P_t} = G_t G_r \left(\frac{\lambda}{4\pi R}\right)^2 \tag{3.1}$$

where P_r and P_t are received and transmit power, respectively; G_t and $G_r$are the antenna gains of the transmitter and receiver gains, respectively; λ is the wavelength and R is the distance from the receiver to the transmitter (in meters). Apparently, it can be generated and calculated directly that, with isotropic antennas ($G_t = G_r = 1$), the effective aperture area decreases with the frequency and the path loss is corresponding to the value of λ. Hence, for mmWave bands with high carrier frequency, the path loss is correspondingly high. However, considering the short wavelength, more antennas can be packed into the same active aperture area and transmitted and received more energy through narrow directed beams with high gains [16, 38, 86]. As indicated in [16], the path loss for propagation with different carrier frequencies, e.g., ranging from3 GHz to 30 GHz, can be the same. Regardless of the frequency, once the physical size and number of antennas are designed applicably, the received power arranged in 30 GHz can even larger than that of the 3 GHz case.

Unlike lower frequency signals, mmWave signals hardly penetrate through most solid materials, such as buildings. In Table 3.1, the attenuation values for common materials are provided by [87, 88]. The signals, when penetrating through buildings will suffer propagation losses, and researches show that signals in lower frequency are more easily penetrating buildings (i.e., with less loss). Moreover, the propagation distance of mmWave is limited, together with the attenuation, will cause a failing transmission from

outdoor to indoor environment. Although some signals may reach inside through windows, the signal is becoming weak and even out of the receiver sensitivity. To solve it, 60 GHz WiFi using mmWave, defined in IEEE 802.11ad, and mmWave femtocell can be installed inside and serve all the inside coverage.

Table 3.1 *Attenuation for different materials [dB]*

		Dry-wall	**Clear glass**	**Mesh glass**	**Wood**	**plasterboard**	**Concrete**
Thickness (cm)	**Carrier frequency**	2.5	**0.3/0.4**	**0.3**	**0.7**	**1.5**	**10**
Attenuation	<3 GHz	5.4	6.4	7.7	5.4	-	17.7
	40 GHz	-	2.5	-	3.5	2.9	175
	60 GHz	6.0	3.6	10.2	-	-	-

Due to the roughly similar size between raindrops and radio wavelengths in mmWave, the presence of rain also causes significant attenuation in mmWave transmission by scattering. As indicated in [78], the category of rain is classified by the rate of precipitation: rate of 0.25mm-1mm per hour stands for light rain; 1mm-4mm per hour means moderate rain; heave rain with rate of 4mm-16mm per hour; very high rain means 16m-50mm per hour. Specifically, for a very heavy rain at the rate of 50 mm per hour, the rain attenuation at 30 GHz carrier frequency is approximately 14 dB/km. The authors in [15, 78] indicate that with 200m of cell coverage as radius in the mmWave communications, the rain attenuation is going to be surmounted and the effect is minimized.

4. EXISTING 5G AND MMWAVE SIMULATORS

Nowadays, a number of organizations and researchers are working on channel modeling in mmWave bands. Regarding of the previous channel models, such as 3GPP-SCM, WINNER models, they can only be partially implemented when combining 5G technology with mmWave. The reasons are basically based on the challenges of path loss, rain attenuation, directivity, and sensitivity to blockage during data transmission [89] and the configuration of antenna arrays, etc.

Due to the higher carrier frequency compared with regular micro-wave, mmWave communications are suffering from huge propagation loss. Theoretically, the free space propagation loss is proportional to the square of the carrier frequency. For example, a 30 GHz mmWave experience around 20 dB path loss more than a 3 GHz signal, according to the Friis free space equation [90]. In this case, the mmWave propagation models are critical for designing proper antennas in regular scenarios for obtaining ideal data rate and the coverage. The authors in [91] indicate that by applying omni-directional antennas, the propagation distance is typically less than 20 meters. Besides, the mmWave with weak diffraction ability, are sensitive to blockage by humans or buildings. The authors in [92] shows, with a propagation measurement in a realistic indoor environment, that the channel blocked time is 1% to 2% of the whole experiment, with the number of person is ranging randomly from 1 to 5. Thus, previous models in UHF band cannot be applied to analyze mmWave networks directly. Additionally, the blockage will cause substantial differences in both NLOS and LOS path loss performances, which also observed in UHF bands [93]. But in mmWave where few clusters exist [94] and the diffraction effects are inappreciable [38], the influence becomes much more significant. Another distinguishing feature when modeling mmWave communication is the propagation environment. MmWave signals suffer penetration loss [95], rain attenuation and atmospheric absorption [96, 97]. Therefore, indoor receivers are unavailable to be covered by outdoor base stations. Furthermore, in mmW-wave communications, large scale antenna arrays are desired in base station and potentially in terminal end for beamforming, in order to compensate the large propagation loss. As indicated in [98], a size of 66mm×66mm plate embedded 1024 antenna elements at E band forms half power beam width to the narrow value of 3 degree.

So far, many geometry based stochastic channel models exist and are widely used. Figure 4.1 illustrates an overview of an evolution about the geometry based stochastic channel models [36]. In 2003, the 3rd generation partnership project (3GPP) spatial channel model (SCM) started. Between 2004 and 2008 the Wireless World Initiative for New Radio (WINNER) projects were developed. The QUAsi Deterministic Radio channel generator (QuaDRiGa) started in 2011. One year later, the mobile and wireless communications

enablers for twenty-twenty (2020) information society (METIS) project was co-funded by the European Commission as an integrated project under the seventh framework program (FP7) for research and development, which later is known as the 3GPP-3D channel model [99]. In this thesis, we will describe in more detail the three models, namely WINNER 2, METIS, and Quadriga, as the ones having the best available documentation and being available, fully or partially, under open-access terms.

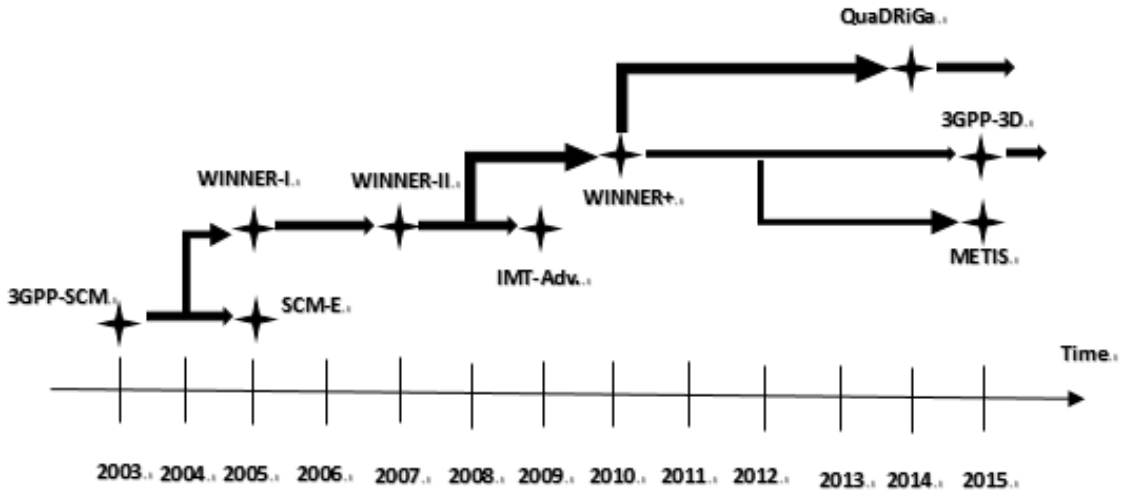

Figure 4.1 *Evolution of geometry-based stochastic channel models [36]*

4.1 WINNER 2

WINNER is a global research project under framework program 6 (FP6) of the European Commission. It develops the new radio interface for systems beyond 3G. As a part of the Wireless World Initiative (WWI), known as a series of cooperating projects in FP6, the objective of WINNER has been to develop a common radio access system which is eligible to general mobile communication scenarios at both short and wide area. The term of WINNER 2 is an extension from WINNER 1 project. As indicated in [100], the radio interface of WINNER 2 supports the requirements beyond 3G. WINNER phase one was developed by the cooperation of several institutions and corporations,namely Elektrobit, Helsinki University of Technology, Nokia, Royal Institute of Technology (KTH), Swiss Federal Institute of Technology (ETH), and Technical University of Ilmenau. At the beginning, the first phase of project was launched based on two standardized models, 3GPP-SCM and IEEE 802.11n. Specifically, 3GPP-SCM and IEEE 802.11n are used in outdoor and indoor simulations, respectively. Moreover, a wideband extension (100 MHz) of bandwidth in WINNER 1 was developed comparing with 5 MHz of it in SCM model. In WINNER 2 project, developed by Elektrobit, University of Oulu / Centre for Wireless Communications (CWC), Technical University of Ilmenau, Nokia, and Communication Research Centre (CRC) Canada, a set of new propagation scenarios and environments, showing in the Table 4.1, were developed, including indoor-to-outdoor, outdoor-to-in-

door, bad urban micro-cell, bad urban macro-cell, feeder link BS-FRS (Fixed Relay Station), and moving networks BS-MRS (Mobile Relay Station), MRS-MS [100]. The extension enabled the original functions with the same channel data in both link and system level simulations. The transceiver techniques, such as coding, modulation and equalization techniques, were added. Overall, the model enhanced in two aspects, including up to 6 GHz frequency range and a number of new scenarios [100,101].

Table 4.1 *New scenarios in WINNER II compared to WINNER I*

Scenario	Definition	LOS/NLOS	Mobility (km/h)	Frequency (GHz)	Concept Group
A2	Indoor to outdoor	NLOS	2-6	2-6	Local Area
B2	Bad urban Microcell	NLOS	0-70	2-6	Metropolitan Area
B4	Outdoor to indoor, microcell	NLOS	0-5	2-6	Metropolitan Area
C3	Bad urban macrocell	NLOS	0-70	2-6	-
D2	BS-MRS rural	LOS	0-350	2-6	Wide Area
	MRS-MS rural	LOS/OLOS/ NLOS	0-5	2-6	Local Area

WINNER channel model is a geometrical stochastic model, which models propagation parameters and antennas separately. Furthermore, the channel parameters are determined stochastically from every single snapshot, and extracted from channel measurement. Practically, antenna geometries and field patterns are all defined by users. The small scale parameters, such as delay, power, angle of arrival (AOA) and angle of departure (AOD), are generated by geometrical principle of rays.

4.1.1 Channel modelling approach

In WINNER project, a cluster is comprised by amounts of rays and the cluster is considered as a propagation path, which diffused in space. The MIMO channel with antenna arrays and propagation paths is illustrated in Figure 4.2.

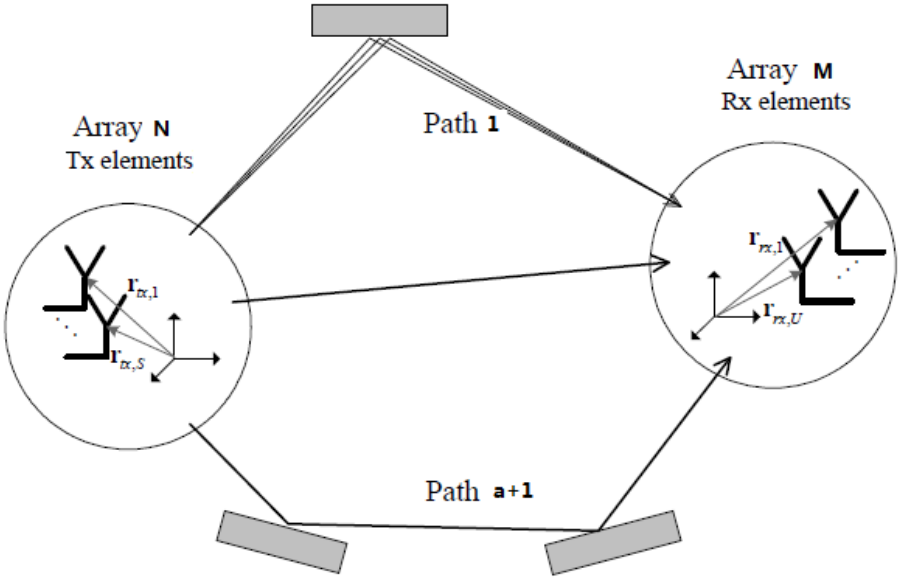

Figure 4.2 *The MIMO channel*

As indicated in [101], the transfer matrix $H(t;\tau)$ for the MIMO channel is

$$H(t;\tau) = \sum_{n=1}^{N} H_n(t;\tau) \tag{4.1}$$

where t is time factor (available for dynamic radio channel), τ represent delay, H_n (with cluster of n) is the channel response matrix, composed with antenna array matrices F_{tx} (transmitter) and F_{rx} (receiver), and it is computed as follows

$$H_n(t;\tau) = \iint F_{rx}(\varphi) h_n(t;\tau,\Phi,\varphi)\, F_{tx}^{T}(\Phi) d\Phi d\varphi \tag{4.2}$$

Specifically, the channel between Tx antenna element s and Rx element u with cluster n is

$$H_{u,s,n}(t;\tau) = \sum_{m=1}^{M} \begin{bmatrix} F_{rx,u,V}(\varphi_{n,m}) \\ F_{rx,u,H}(\varphi_{n,m}) \end{bmatrix}^{T} \begin{bmatrix} a_{n,m,VV} & a_{n,m,VH} \\ a_{n,m,HV} & a_{n,m,HH} \end{bmatrix} \begin{bmatrix} F_{tx,s,V}(\Phi_{n,m}) \\ F_{tx,s,H}(\Phi_{n,m}) \end{bmatrix} \times \exp\left(j2\pi\lambda_0^{-1}(\bar{\varphi}_{n,m} \times \bar{r}_{rx,u})\right) \times \exp\left(j2\pi\lambda_0^{-1}(\bar{\Phi}_{n,m} \times \bar{r}_{tx,s})\right) \times \exp(\mathrm{j}2\pi v_{n,m}\mathrm{t}) \times \delta(\tau - \tau_{n,m}) \tag{4.3}$$

where u and s are the antenna elements, and $F_{rx,u,V}$ and $F_{rx,u,H}$ mean the field patterns for vertical and horizontal polarizations. Moreover, $\bar{\varphi}_{n,m}$ and $\bar{\Phi}_{n,m}$ are AOA and AOD unit vectors respectively. The $a_{n,m}$ represents the complex gain, while VH is the transition from vertical to horizontal, vice versa. Also $\bar{r}_{tx,s}$, $\bar{r}_{rx,u}$ are the location vectors, and $v_{n,m}$ is the Doppler frequency component of ray n and m.

4.1.2 Modelling process

The process of modelling WINNER 2 channel is divided into three segments. The first part is started by defining the propagation scenarios, such as the environment, the antenna

parameters, and network layout. The second part consisted of the data analysis, and the last step was about the channel model realization, as indicating in Figure 4.3. The diagram illustrates all the procedures including defining the general parameters, especially for the Large Scale Parameters (LSRs) of delay spread (DS), angle spread (AS), shadow fading (SF) and K factor. Then, the small scale parameters through channel measurements are generated. And last, there is coefficient generation.

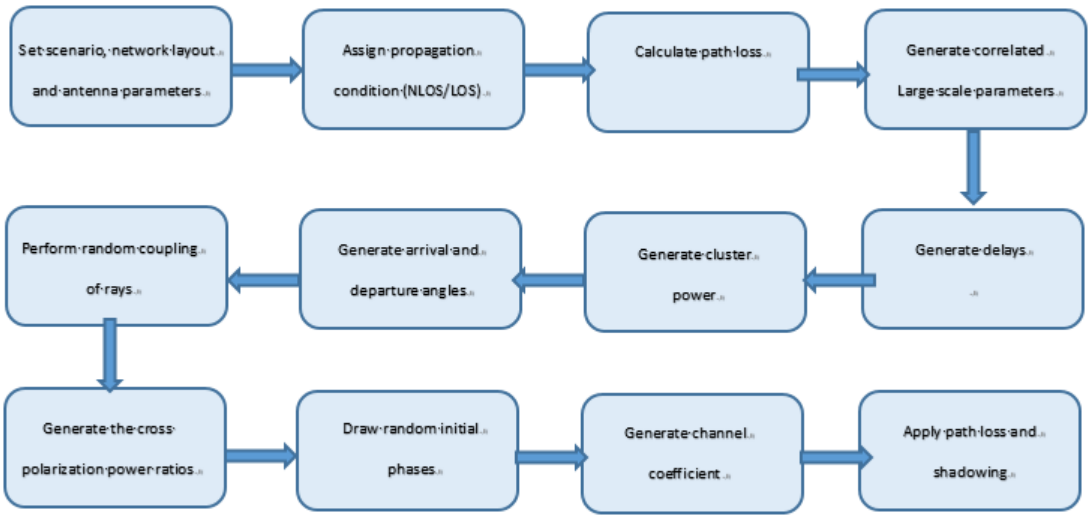

Figure 4.3 *WINNER 2 channel modelling process*

In term of the network layout, it has to be noted that, WINNER models enables both link and system level simulations. In this case, multiple links can be simulated simultaneously. Figure 4.4 shows that system level simulation contains multiple base stations, relay stations and terminals. Also in this picture, each short blue line stands for a channel segment with fixed LSRs. And the dashed line area means a link level simulation.

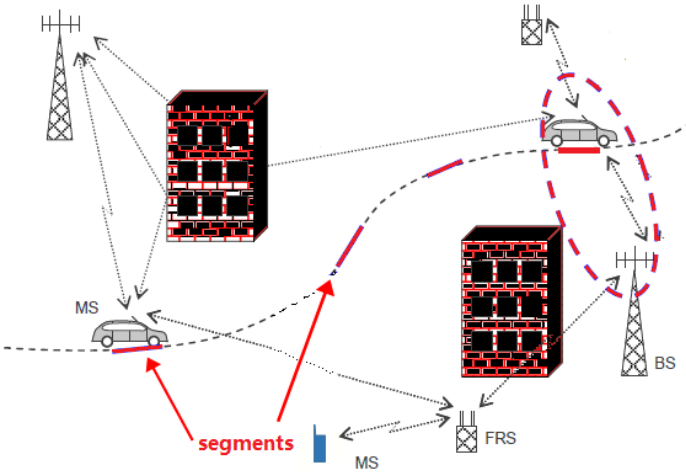

Figure 4.4 *System level approach*

Comparing to models of cluster level approach, the geometrical stochastic WINNER 2 channel model [100, 102] follows a system level approach. As mentioned, WINNER 2

channel model can be conducted at both link level and system level for the evaluation of wireless systems. The model also supports multi-antenna technologies, polarization, multi-user, multi-cell, and multi-hop networks.

4.2 METIS

While conventional channel models such as SCM, WINNER, and International Mobile Telecommunications-Advanced (IMT-Advanced) were implemented for frequencies up to 6 GHz, other models such as IEEE 802.11ad particularly support the 60 GHz band. Due to actuality, the METIS channel model was designed to deal with the full frequency range from cellular bands of below 6 GHz up to 86 GHz [103].

METIS, known as Mobile and Wireless Communications Enablers for Twenty-twenty (2020) Information Society, is a project co-funded by the European Commission as an Integrated Project under the Seventh Framework Program (FP7) for applying 5G technology into commercial and industrial worlds. As described in [104], since none of the existing channel models such as WINNER, IMT-Advanced, COST 2100, and IEEE 802.11 fully fulfill all the 5G network requirements, the ultimate goal for METIS is to satisfy the particularly envisioned 5G scenarios and test cases. The original requirements as planned include the highly wide frequency range from 86 GHz to beyond, very high bandwidths around 500 MHz, completely 3D version, large array antennas, and dual-mobility for D2D, etc. Basically, the METIS channel models contain three types, including a map-based model, a stochastic one and a hybrid channel model, which is combined by the former two models. The comparison between the various METIS models, given in [104] is reproduced in the Table 4.2. Particularly, the map-based model applies ray tracing and describes the propagation environment in a three dimensional geometric way. Thereby, the model illustrates the propagation mechanism clearly, such as diffraction, regular reflection, diffuse scattering, blocking, and supports precise channel properties for realizing massive MIMO, advanced beamforming and path loss modeling. On the other side, the stochastic model is developed from the GSCM, WINNER for the objective of enabling multiple dimensional shadowing maps with low complexity, millimeter wave parameters, power angular spectrum sampling and so on. As a combination of the hybrid model, it generates a flexible model framework in balancing the simulation complexity and realism. As an example given by [104], "*shadowing attenuation may be based on a map while small-scale fading is stochastic*"

Table 4.2 *Comparison of models in METIS*

	METIS Model		
	Stochastic	Map-based	Hybrid
Center Frequency	up to 70 GHz	up to 100 GHz	up to 70 GHz
Bandwidth	100 MHz < 6 GHz 1 GHz @ 60 GHz	10 % of the center frequency	100 MHz < 6 GHz 1 GHz @ 60 GHz
Pathloss	separate, empirical	implicit	implicit
Shadowing	separate	implicit	implicit
Parameterization by measurements	easy	easy	easy
Massive MIMO	limited	yes	limited
Spherical waves	no (except the luster location is fixed)	yes	no (except the luster location is fixed)
3D	yes	yes	yes
Millimeter wave	partly	yes	partly
Dynamic modelling	no	yes	no
Polarization modelling	XPR	Ray-based	XPR
Public implementation available	no	no	no

4.2.1 Propagation scenarios and test cases

The scenarios depict an internally consistent view of what the future might turn out to be [105], and summarize the scope of METIS from end-user perspective, also illustrate a specific challenge. Defined by METIS, five generic propagation scenarios (PSs) [106] are described for the fundamental challenges of the 5G mobile systems. There are:

- Scenario 1: Amazingly fast to reflect the very high data rate challenge
- Scenario 2: Great service in a crowd to address the challenge of very dense crowds of users
- Scenario 3: Ubiquitous things communicating to represent very low energy, cost, and a massive number of devices challenge
- Scenario 4: Best experience follows you to address the mobility challenge

- Scenario 5: Super real-time and reliable connections to set the very low latency challenge

Moreover, twelve test cases (TCs) [106] are defined by covering the veritable applications of 5G system, while each of TC contains the assumption, constraint and requirements, and belonging to several scenarios. TCs are listed below in Table 4.3.

Table 4.3 *METIS Test Cases (TC)*

TC	Definition
1	Virtual Reality Office
2	Dense Urban Information Society
3	Shopping Mall
4	Stadium
5	Teleprotection in smart grid network
6	Traffic Jam
7	Blind Spots
8	Real-time remote computing for Mobile Terminals
9	Open Air Festival
10	Emergency Communications
11	Massive Deployment of Sensors and Actuators
12	Traffic Efficiency and Safety

4.2.2 Modelling approach

Since the stochastic channel models in METIS follow the similar principles as in WINNER 2, the map-based model is developed for realizing spatial channel properties. And it is based on ray-tracing, realizing the propagation modelling with low complexity, especially in a simple and symmetrical map such as Manhattan and Madrid grid of TC 2. More specifically, the procedure of METIS map-based modeling can be divided into four sections, shown in Figure 4.5.

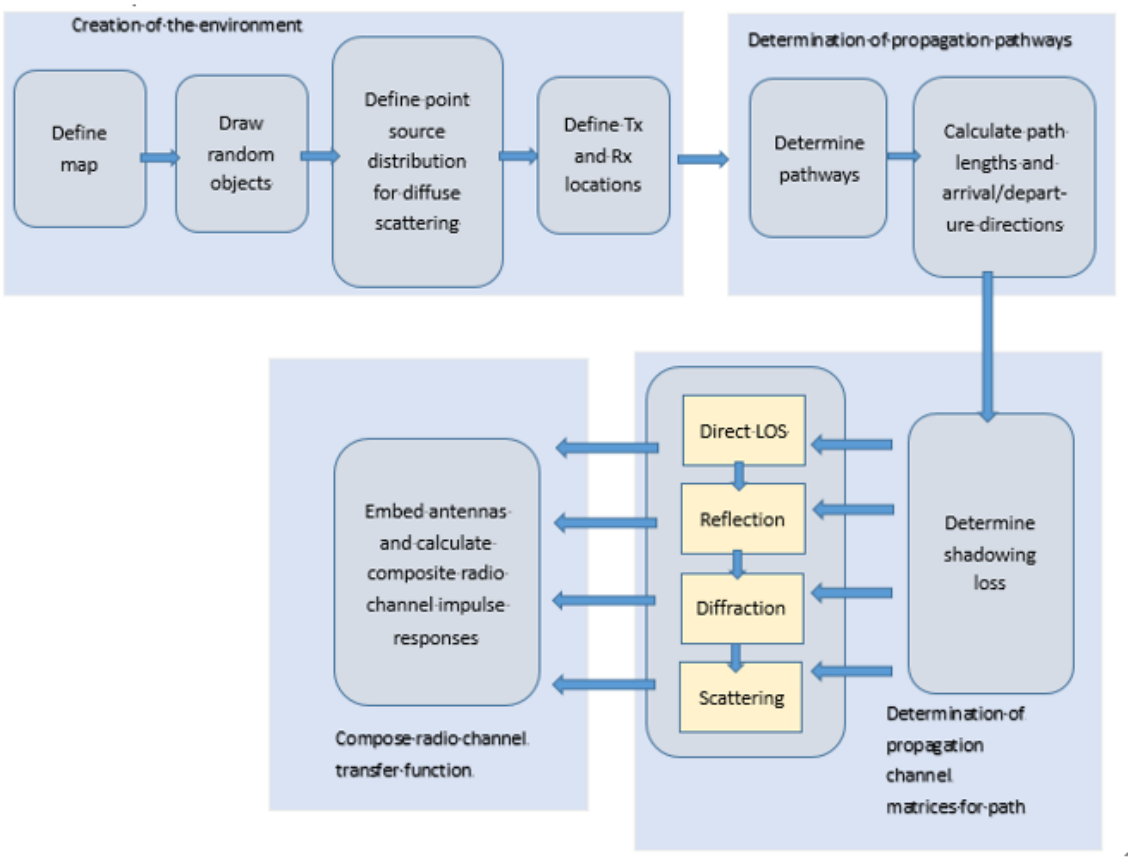

Figure 4.5 *METIS map-based modeling diagram*

In terms of creation of the environment, for METIS scenario of Manhattan (PS 1 and 2), the first step is to define the map in global coordinate system. For instance, the user and allocate the building of length and width with X and Y coordinates, respectively and the height in Z axis. Then, the user initiates the shadowing and scattering objects by defining the coordinates in X, Y, Z, according to some known regular pattern, for example the windows or seats indoor, or by drawing randomly from the uniform distribution [104] as

$$\mathrm{o}_n(x, y, z) = (X_n, Y_n, Z_n) \tag{4.4}$$

where $X_n \sim U(0, X_{max}), Y_n \sim U(0, Y_{max}), Z_n = 1, n = 1, \ldots (X_{max} Y_{max} \mathrm{D}), X_{max}$ and Y_{max} are the edges of the map on x and y axis, respectively. D means the different distribution densities, which depends on various scenarios. The distribution densities should follow the rule not staying too close, for example closer than half of the object width. And the shadowing screen size is relevant to the object height and width, such as vehicles, trees and humans. In PS 1 and 2, the parameters are given as object height (1.5/4), object width (0.5/3) [104]. Once considering the moving cases, the trajectory and speed of motion have to be defined separately. The next step is to define the point source distributions, which are corresponding to the density according to the antenna angular resolution requirement. Practically, the center points of the tiles can be calculated as below (the tile centers are parted in vertical direction and in horizontal direction)

$$\begin{cases} N_z = \left\lceil \frac{wall\ height}{\sqrt{\Delta s}} \right\rceil \\ N_{xy} = \left\lceil \frac{wall\ width}{\sqrt{\Delta s}} \right\rceil \end{cases} \tag{4.5}$$

where Δs is the high limit of tile area. The x coordinates of tile centers are calculated by dividing the x coordinates of the wall to N_{xy} equal parts and taking each of the center parts as x coordinate of a tile. Also the y and z coordinates follow the same method by the given parameter of N_{xy} and N_z, respectively. As a consequence, the new tile area can be determined as

$$\Delta s = \frac{wall\ height \cdot wall\ width}{N_{xy} N_z} \tag{4.6}$$

Normally, the first three steps are just implemented once, then the whole procedure is completely deterministic. In the next step, starting by defining the transmitter and receiver locations, multi-radio links, which are corresponding to the specified environment through former three steps are modelled coherently by repeating next steps. In the single radio link case, the position vectors of antenna in transmitter (elements of s) and receiver (elements of u) are

$$\begin{cases} r_u^{Rx} = [x_u \quad y_u \quad z_u]^T \\ r_s^{Tx} = [x_z \quad y_s \quad z_s]^T \end{cases} \tag{4.7}$$

where u=1,…, U and s=1,…,S. U and S represent the number of antenna elements.

In the second section of the procedure, the objective is to determine propagation pathways. According to the METIS map-based model concept, all possible secondary nodes with a LOS path are visible to the transmitter and receiver, as well as via a single regular reflection. Normally, the possible secondary nodes can be corners, scattering objects and sources. Consequently, the coordinates and reciprocal points can be determined, as well as the pathway can be recognized as blocking by wall directly or reflected. After that, the progress is repeated and complete amount of reflection and diffraction interaction by starting from defining the transmitter and receiver positions. As a result, a set of vectors $\psi_k=\{\psi_{ki}\}=\{x_{ki,}y_{ki,}z_{ki,}T_{ki,}\}$, k=1,…, k, i=1,⋯, I_k is generated, where K and I_k mean the number of pathways and path segments, respectively. $x_{ki,}y_{ki,}z_{ki}$ are the coordinates in x, y and z axis of i^{th} interaction point of K. T_{ki} means the type of interaction, contains direct, reflection, diffraction, and scattering.

In the 6th step, the direction of arrival and departure for K paths are determined as a wave form of vectors, such as $K_{k,u,s}^{Tx}$ and $K_{k,u,s}^{Rx}$. The vectors are pointing from transmitter to the starter of interaction point and from the end interaction point to receiver, respectively. Continuously, the length $d_{k,i,u,s}$ for every single segment of path k is calculated by applying Euclidean distance. And the transmission delay is $\tau_{k,u,s}=d_{k,u,s}/c$ (c is the speed of light), the total path length is

$$d_{k,i,u,s} = \sum_{i}^{I_k} d_{k,i,u,s} \tag{4.8}$$

In terms of the shadowing caused by blocking objects, Figure 4.6 illustrates approximately a rectangular screen case. The screen is installed in vertical and perpendicular direction while two nodes connect through the links, which provide two types of view. The shadowing loss can be modelled by a simple knife edge diffraction model [107] as

$$L_{sh|dB} = -20\log_{10}((1-(F_{h1}+F_{h2})(F_{w1}+F_{w2})) \tag{4.9}$$

where $F_{h1}, F_{h2}\ and\ F_{w1}, F_{w2}$ account for diffraction at four edges referring to the height and width. For every single edge of shadowing, it is

$$\mathrm{F} = \frac{\mathrm{atan}(\pm\frac{\pi}{2}\sqrt{\frac{\pi}{\lambda}(D_1+D_2-r)})}{\pi} \tag{4.10}$$

where D_1, D_2 are the distances between the nodes and screen surface, λ is the wave length and r represents the distance between the transmitter and receiver

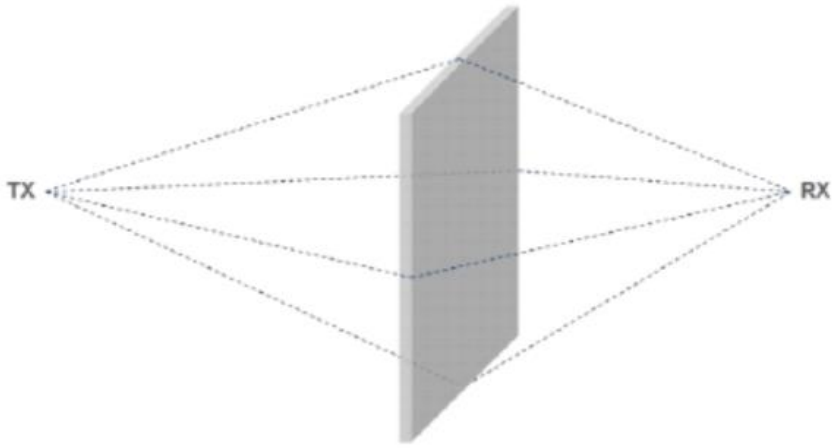

(a)

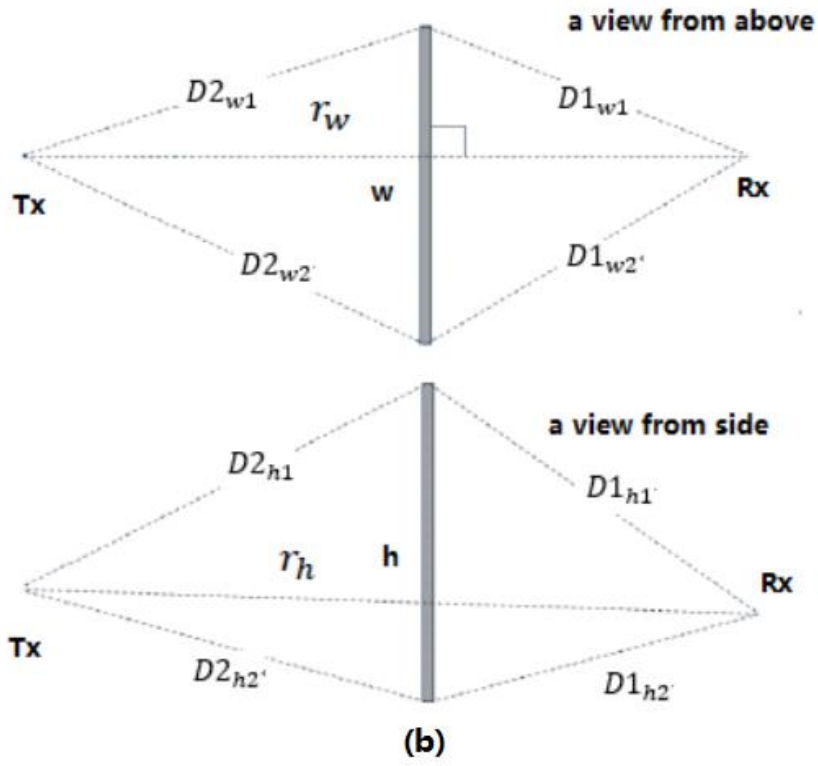

Figure 4.6 (a) *Shadowing screen model* ***(b)*** *Different views from above and side*

For a dense distribution case of screens, such as open air festival scenario, the sum of pathlosses due to multi-screens will generate unreasonable superabundant loss. Thus, the blocking model of Walfisch-Bertoni [108] can be supplemented. As shown in Figure 4.7, the main shadowing screen is adjacent to the Rx. The shadowing L_{sh} of this screen follows knife edge diffraction model. After that, the additional loss corresponding to the multi-screen is generated

$$L_{md|dB} = -20\log_{10}(2.35g_p^{0.9}),\ g_p = \frac{\theta}{\theta_o}\sqrt{\frac{d}{\lambda}} \tag{4.11}$$

where θ_o is 1 rad, θ (varies from 0 to $\pi/2$) represents for the elevation angle between the main screen of upper edge to the Tx, d is the average distance among the screens. The total shadowing loss is

$$L_{sh\_tot} = L_{sh|dB} + L_{md|dB1} \tag{4.12}$$

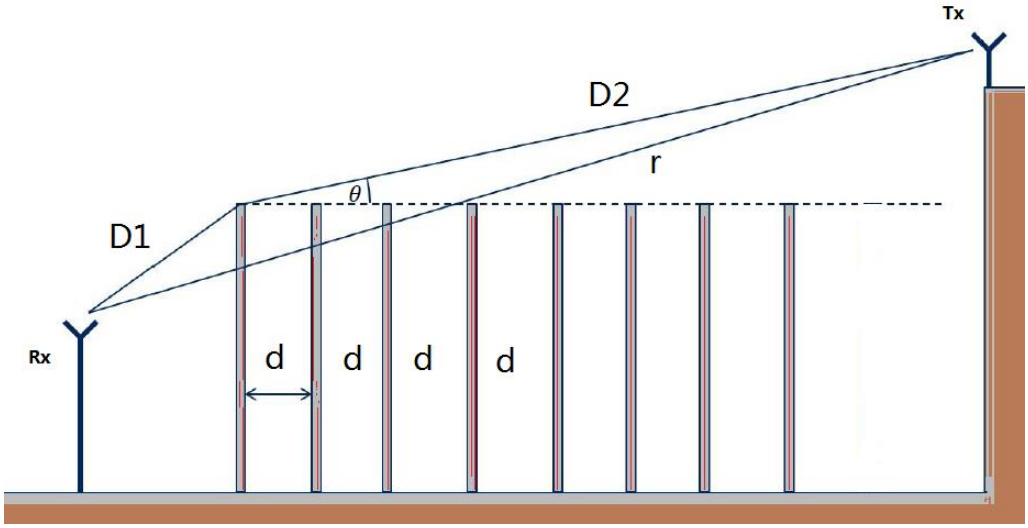

Figure 4.7 *Shadowing of multi-screen*

In another case [104], both the height of transmitter and receiver are low, showing in the Figure 4.8. The angle is

$$\theta = \frac{\max(h_{off}; h_{Tx} - h_{sc})}{D2_{Rx}} \theta_o, h_{off} = (2.35 \frac{d}{\lambda}^{-0.9} d_o) \quad (4.13)$$

The loss related to the screens which are closest to Rx and Tx are multiplex to the multi-screen loss, as

$$L_{sh\_tot|dB} = L_{sh\_tx|dB} + L_{sh\_rx|dB} + L_{md|dB} \quad (4.14)$$

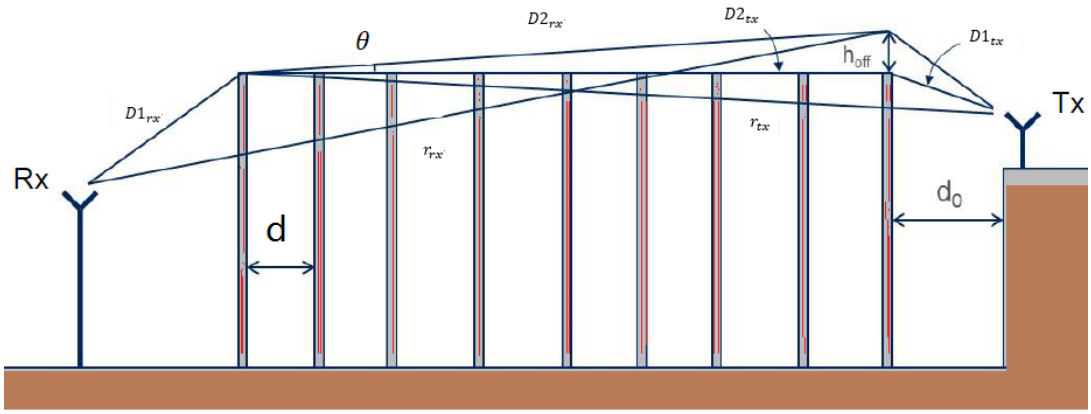

Figure 4.8 *Shadowing model case with lower Tx and Rx*

Furthermore, a 2×2 matrix of polarization transfer for the LOS path segments k and i is given

$$h_{k,i,u,s} = \begin{bmatrix} 1 & 0 \\ 0 & -1 \end{bmatrix} \quad (4.15)$$

and the divergence factor of LOS path F^{LOS} equals to $1/d_{k,i,u,s}$. Relating to all path segments (with regular reflection), the 2×2 matrix is

$$h_{k,i,u,s} = \beta A^{ref}_{k,i,u,s} \tag{4.16}$$

where i is the number of nodes, β is the ratio power of reflection and scattering, whose value is availably set as 0.5 by [104]. Overall, from the METIS deliverable D1.4, we can get the brief complex impulse response (CIR) between transmitter and receiver antennas (with motion of transceivers)

$$H_{u,s}(\mathrm{t},\tau) = \sum_{K=1}^{K} g_u^{Rx}\left(-k_{k,u,s}^{Rx}(t)\right)^T e^{\frac{j2\pi d_{k,u,s}(t)}{\lambda}}\left(\prod\nolimits_{i=1}^{I_k} h_{k,i,u,s}(t) F_{k,i,u,s}^{T_{ki}}(t)\right) g_s^{Tx}\left(k_{k,u,s}^{Tx}(t)\right) \delta(\tau - \tau_{k,u,s}(t)) \tag{4.17}$$

where g_u^{Rx} and g_s^{Tx} are vectors of the complex polarimetric antenna pattern, $F_{k,i,u,s}^{T_{ki}}$is the divergence factor according to the path segment. In Berg recursive option [133], $F_{k,i,u,s}^{T_{ki}} \equiv 1$ for pathways with diffraction. The parameter t is exchangeable for parameters relating to the Tx and Rx locations (with moving speed, except for the scattering kinetic object which has time dependent coefficients but temporal variation independent Rx and Tx locations).

In a conclusion, according to [109], the model can be simplified by accounting only for diffracted paths, which are in a lower order of Fresnel zones is referring to the matching specular and direct path. Specifically, the diffracted path should be considered while the specular and direct paths are shadowed. For more details see [109]. In addition, the objective of METIS map-based model is implemented for all radio channel characteristics. So far, most of the properties have already been successfully fulfilled with results and outcomes as demonstrated according to the METIS deliverables.

4.3 QuaDRiGa

QuaDRiGa was developed in the year of 2011 by the Fraunhofer Heinrich Hertz Institute within the Wireless Communications and Networks Department, with the partner European Space Agency. The main objective was to enable the modeling of MIMO radio channels for the decided network configurations, such as indoor, satellite and heterogeneous. The work was supported by the European Space Agency (ESA) in the Advanced Research in Telecommunications Systems (ARTES) program, the German Federal Ministry of Economics and Technology (BMWi) in the national collaborative project IntelliSpektrum, the European Commission co-founded the project METIS as an Integrated Project, the GreenTouch consortium within the funded project "LSAS Channel Modelling", and the European Commission co-founded the project millimeter-MAGIC as an Integrated Project.

It is known that channel models are crucial methods to estimate the performance of updated concepts in mobile communications. QuaDRiGa, as an enhancement of the WINNER model, also follows a stochastically geometry based channel modelling approach, and it can be comprehensively considered as a WINNER model in a full 3D version with extension requirements for satellite propagation scenarios. Comparing with WINNER models, several new features are originally ongoing to implement, such as

- *Time evolution*. The channel coefficients of short-term time evolution is implemented with the updating delays, arriving angel, departing angle, polarization, shadow fading, and K-factor.
- *Scenario transition*. Considering that user terminals move through fading channels within several scenarios for long-term time evolution, QuaDRiGa provides smooth transitions between nearby segments.
- *Variable speeds for mobile terminals*. Accelerating and slowing down of user terminals.
- *Common framework for NLOS and LOS simulations*. Same method for LOS and NLOS scenarios which decreases the complexity and implements free multi-cell scenarios.
- *Geometric polarization.* Both of NLOS and LOS polarizations are calculated based on ray-geometric approach.
- *Improved method for calculating correlated LSP*. Using filtered random numbers to generate maps of correlated parameters, and enhancing the algorithm for off-angle movement directions.
- *New functions for modifying antenna patterns*. Antenna patterns are rotated in 3D coordinate.

In QuaDRiGa, an arbitrary two-way direction radio channel was created. And the model is antenna independent, while the configuration and element patterns are defined manually. The channel parameters based on statistical distribution are extracted from channel

measurements. Meanwhile, the distribution of DS, delay value, AS, SF and XPR are defined. Specifically, the channel is generated by rays with parameters, such as delay, power, AOA, and AOD. Different parameters result various scenarios through the same approach. The modelling approach features are listed [36]:

- Free configuration of network layouts with multi-transmitter and multi-receivers
- Same modeling approach, as well as satellite scenarios
- Various frequencies bands for modeling while setting available parameters
- Eligible for multiple antennas technology, polarization, multiple users, and multiple hop networks
- 3D dimension of antennas and propagation scenarios (the importance of a 3D extension for researching cross-polarized antennas on MIMO capacity is indicated in [110].)
- Available for massive MIMO antennas at BS and MS

Unlike the typical ray racing approach, in QuaDRiGa it can be considered as a statistical ray tracing model with distributing scatterer positions randomly. As illustrated in Figure 4.10 with a simple example of only two paths, a scatterer is present and it creates an NLOS component. For every single path, the model is built with AOD, AOA and the total path length. Basically, each circle of a scatterer with several dots represents a scattering region causing one cluster, which is modeled by an individual reflection. Normally, 20 dots, containing in the scatterer as sub-paths, are combined into a signal and represent a path. In a rich scattering environment, the angular spread increases as well as the number of scattering clusters. Thus, QuaDRiGa provides up to 42 clusters. Normally, the amount of discrete clusters depending on AS and diffuse scattering are around to 10 and for LOS propagation and 20 for NLOS propagation, respectively.

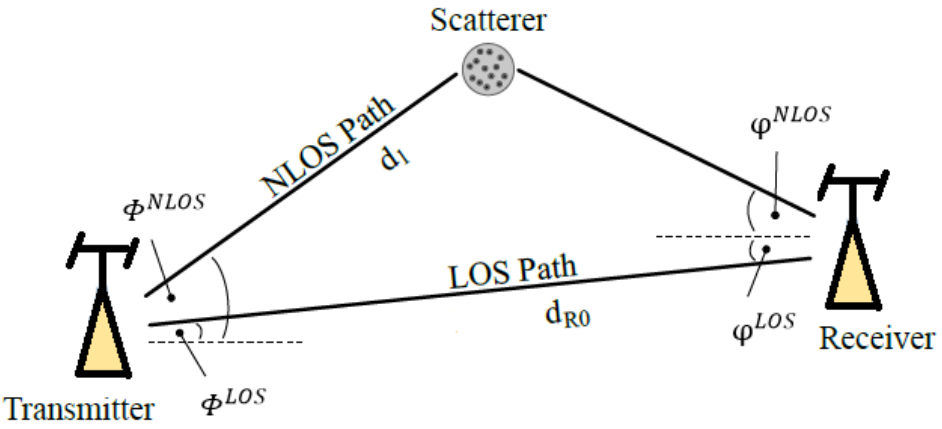

Figure 4.10 *Overview of simple modeling approach*

4.3.1 Modelling approach

From the general perspective of QuaDRiGa, the modeling approach consists of two steps, including generating LSPs stochastically and calculating the 3D positions of scattering clusters randomly. In Figure 4.11, it illustrates a particular procedure. For every propagation environment, such as urban, suburban, and rural, the channel performance is presented in terms of the statistic LSPs, which are inserted manually, such as DF, AS, SF, and Ricean K-factor. Additional parameters, such as the decorrelation distance, illustrate the quick changes of channel.

When modelling QuaDRiGa practically, the model starts by configuring the network layout, which including transmitter position (satellite orbital positions are available in QuaDRiGa), antenna properties at both transmitter and receiver, user terminal trajectory, the scenarios along the trajectory, and assigning a propagation environment for each scenario. Both the trajectory and scenarios are performed by the state sequence generator (SSG) [36], which supports manual definition of all parameters and measurement of trajectory and scenario sequence from data. The trajectory accounts for the position of the mobile terminal. And for the scenarios assigning along the trajectory, clusters are measured in accordance with LSPs. Every single cluster is divided into 20 sub-paths, with the calculated corresponding AOA, as well as for the position of user terminals along the trajectory. Then, the phases are measured according to the position of the terminal antennas, which is corresponding to the clusters. And the terminal trajectory describes how the phase changes in Doppler spread. Additionally, the MIMO channel response is created after summing up the coefficients of 20 sub-paths. The channel coefficients of adjacent scenarios are merged, where the progress contains the birth and death of clusters, [111] introduced more research as well as the lifetime of individual scattering clusters [112]. After all, all the channel coefficients combing with the path delays are generated and for further analysis.

During the modeling approach, the time evolution requires a particular description of the terminal mobility, which is supported by assigning tracks to every mobile terminal. In practical scenarios, acceleration, decelerations and velocity to pedestrians and vehicles are also included. Thus, in order to calculate the channel coefficients, [113] states a constant sample rate which is fulfilled the sampling theorem and used to minimize the computation and internal storage

$$f_T \geq 2B_D = 4max|\Delta f_D| = 4\frac{max|v|}{\lambda_c} \tag{4.18}$$

where B_D is the Doppler spectrum width, Δf_D is the maximum change of frequency corresponding to the velocity v, and λ_c is the carrier wavelength. Therefore, the suitable sampling rate is relative to the peak speed of the terminal.in a normalized manner knowing as sample density (SD), a temporal sequence for varing speeds is measured by manipulate the coefficients in post-processing:

$$f_S = \frac{f_T}{max|v|} \geq \frac{4}{\lambda_c} \tag{4.19}$$

$$SD = \frac{f_S}{\lambda_c/2} \geq 2 \tag{4.20}$$

where f_S is the sampling rate measuring in samples per meter.

In details, the modeling approach is illustrated in the Figure 4.11. In the diagram of the grey parts are changes made from WINNER, including departure and arrival angles, drifting, polarization of channel coefficients, and transitions between scenarios. When calculate four angles for clusters, the additional elevation angle of departure θ^d and arrival θ^a are added in QuaDRiGa. The angles are calculated in the same method but with different angular spread σ_Φ. Thereby, the parameter of σ_Φ represents for σ_{Φ^a}, σ_{Φ^d}, σ_{θ^a} and σ_{θ^d} in the following equations. Assuming that the power angular spectrum in a wrapped Gaussian distribution for all clusters [101, 114]

$$\mathrm{P}(\Phi) = \frac{1}{\sigma_\Phi\sqrt{2\pi}}\exp\left(\frac{-\Phi^2}{2\sigma_\Phi^2}\right) \tag{4.21}$$

and function $C_\Phi(L,K)$ correct he variance to ensure σ_Φ is correctly reflected in the measured angles

$$C_\Phi(L,K) = \frac{1}{\sigma_\Phi^{max}}\int_0^{\sigma_\Phi^{max}} \frac{\bar{\sigma}_\Phi(\sigma_\Phi)}{\sigma_\Phi} d\sigma_\Phi \tag{4.22}$$

where L $\in |2,42|$ and K $\in |-20,20|$ [112], σ_Φ is dependent of $\bar{\sigma}_\Phi(\sigma_\Phi)$ which generated from the individual angles of Φ_l. While neglecting the scaling factor $1/\left(\sigma_\Phi\sqrt{2\pi}\right)$, the angle Φ_l is obtained through normalizing the power angular spectrum

$$\Phi_l = \frac{\sigma_\Phi}{C_\Phi(L,K)}\sqrt{-2\ln(P_l/\max(P_l))} \tag{4.23}$$

The next step is creating two random parameters, X_l and Y_l, where X_l ranges from {-1, 1} as plus and minus sign, $Y_l \sim \mathrm{N}(0,\ 0.01\cdot \sigma_\Phi^2)$.. Then

$$\Phi_l^{[2]} = X_l \cdot \Phi_l + Y_l \tag{4.24}$$

$\Phi_l^{[2]}$ exceeds ±π while the power of a path is less than the peak one, and the changes to

$$\Phi_l^{[3]} = (\Phi_l^{[2]} + \pi \bmod 2\pi) - \pi \tag{4.25}$$

Considering the elevation spreads, possibly ranging from -π/2 to π/2, the correct values of $\Phi_l^{[3]}$ is modified

$$\Phi_l^{[4]} = \begin{cases} \Phi_l^{[3]}, & for\ el.\left|\Phi_l^{[3]}\right| < \frac{\pi}{2}\ and\ all\ az.angles \\ \pi - \Phi_l^{[3]}, & for\ elevation\ \Phi_l^{[3]} > \frac{\pi}{2} \\ \Phi_l^{[3]} - \pi, & for\ elevation\ \Phi_l^{[3]} < -\frac{\pi}{2} \end{cases} \tag{4.26}$$

Finally, each cluster in NLOS are divided into 20 sub-paths to simulate intra cluster AS, while no sub-paths in LOS.

$$\Phi_{l,m} = \Phi_l^{[4]} - \Phi_1^{[4]} + \Phi^{LOS} + c_\Phi \cdot \widehat{\Phi}_m, \quad for\ l > 1 \tag{4.27}$$

where m is the order of sub-path, c_Φ means the root mean square (RMS) angular spread and $\widehat{\Phi}$is the offset angle corresponding to the sub-path. Moreover, the pair of angles ($\theta_{l,m}^d$,$\Phi_{l,m}^d$) at transmitter coupled with random angles ($\theta_{l,m}^a$ $\Phi_{l,m}^a$) at receiver.

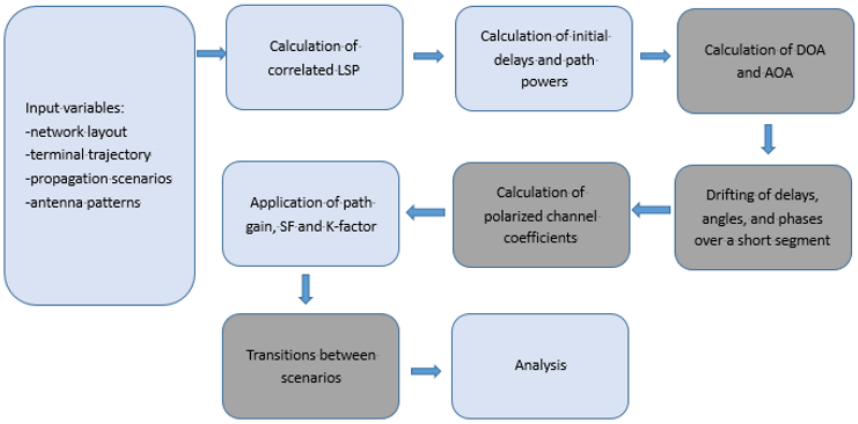

Figure 4.11 *QuaDRiGa channel modeling diagram*

Continuously, [36] indicates combining the antenna patterns, polarization and phases into the measurement of channel coefficients for the scenario snapshots. The 3D polarimetric F is defined for antennas, including vertical and horizontal polarization

$$\mathrm{F}(\theta, \Phi) = \begin{pmatrix} F_V(\theta,\Phi) \\ F_H(\theta,\Phi) \end{pmatrix} \tag{4.28}$$

The antenna gains from transmitter and receiver antennas is calculated previously among departure and arrival angels, then the coefficient

$$g^{[1]}_{r,t,l,m,s} = F_r(\theta^a_{r,l,m,s}, \Phi^a_{r,l,m,s})^T \cdot M \cdot F_t(\theta^d_{t,l,m,s}, \Phi^d_{t,l,m,s}) \tag{4.29}$$

Normally, the changes of polarization corresponding to the propagation path is captured by the matrix M, while WINNER models use random coefficients to deal with the effects. As explained in [115], the random coefficients cannot account for all polarization effects in MIMO radio link. Thereby, M matrix based on linear transformation is proposed in QuaDRiGa. Due to multipath component of initial phase ψ^0, a random cluster power is generated by summing of 20 sub-paths. Normalizing the first sum of complex phase and averaging the power among all S scenario snapshots, the channel coefficients are updated

$$\psi^+_{r,t,l,m,s} = \exp(-j\psi^0_{l,m} - j\psi_{r,t,l,m,s}) \tag{4.30}$$

$$g^{[2]}_{r,t,l,s} = \sqrt{\frac{P_t}{\beta}} \cdot \sum_{m=1}^{20} g^{[1]}_{r,t,l,m,s} \cdot \psi^+_{r,t,l,m,s} \tag{4.31}$$

$$\beta = \frac{1}{S}\sum_{s=1}^{S}\left(\sum_{m=1}^{20} \psi^+_{r,t,l,m,s}\right)^2 \tag{4.32}$$

where P_t is the initial power of each cluster.

Generally, the calculation of initial delays and cluster powers, DOA and AOA, and polarization coefficients, and application of path gain, SF and K factor are independent for scenarios of the mobile terminal trajectory. In QuaDRiGa, those segments are combined

into a long time-evolving sequence of channel coefficients for the purpose of transition between scenarios. The path power of old segment is decreasing and a new one from other segment is increasing. Furthermore, the region is split into several subintervals, as modeling the power ramps

$$\omega^{[sin]} = sin^2\left(\frac{\pi}{2} \cdot \omega^{[lin]}\right) \tag{4.33}$$

$\omega^{[lin]}$ is a linear ramp range belonging to (0,1), and $\omega^{[sin]}$ is a sinusoidal ramp with an invariable slope at both start and end of the overlapping. In LOS, the clusters at both segments are the same and only power and phase need to adjust. In order to minimize the effect for the instantaneous LSPs value, clusters have to be matched carefully. For instance, a strong cluster ramps down with a large delay and a similar cluster with a small delay ramped up, the DS decreases. To avoid the fluctuation, the clusters from both segments are paired, which is supported by calculating the DS at the beginning and ending of the transition.

In QuaDRiGa, the model extended the popular WINNER channel model with new features and allowed freely configuration to the network layouts with multi-transmitters and multi-receivers. The scalability covers from single link, single antenna to heterogeneous multi-link MIMO scenarios. Furthermore, the model was implemented a new polarization model [113] and was merged by the same method to calculate both LOS and NLOS channels, while WINNER implemented different ways. All the existing WINNER parameters showing in the deliverables are available for using in QuaDRiGa, which allow to conduct virtual trials in some new scenarios.

4.4 Comparison among the main existing mmWave channel models

Nowadays, there are several channel models including 3GPP-SCM, WINNER I, WINNER II, COST 2100, IMT-Adv., IEEE 802.11ad, QuaDRiGa, and METIS etc. With the explosively growing of demand in high data rate transmission, channel modeling as crucial method for evolution and trials in wireless communication is prosperously boosted. Specially, when entering into the 5G era, the 5G channel models are emerged one by one. Here Table 4.4 and Table 4.5 illustrate the comparison among most of the popular models in both literature and technical ways.

Table 4.4 *Literature comparison*

	3GPP-SCM	**WINNER I**	**WINNER II**	**COST-2100**	**IMT-Adv.**	**QuaDRiGa**	**METIS**
Accessibility	Open source	Open source	Open source	Licensing condition	Licensing condition	Open source	Licensing condition
Released	2003	2005	2006	2007	2008	2012	2015
Ease of use	Medium	Good	Good	Low	Low	Good	Good
Available documentation	Low level of detail	Very detailed	Very detailed	Low level of detail	Low level of detail	Very detailed	Low level of detail
2D or 3D	2D	2D	2D	2D	2D	3D	3D
References	[116,111,118]	[119,120,121]	[100,101,128]	[122,123,124]	[125,126,127]	[36,113]	[103,104,106]

Table 4.5 *Technical comparison*

				METIS		
Feature	**3GPP SCM**	**IMT-2100**	**IEEE 802.11ad**	**Stochastic**	**Map-based**	**QuaDRiGa**
Frequency-Range (GHz)	1-3	1-6	0.45-6	60-66	Up to 70	Up to 100
Bandwidth (MHz)	5	100	100	2000	100 MH < 6 GHz 1 GHz @ 60 GHz	10% of the Center frequency
Massive MIMO	No	limited	No	Yes	Limited	Yes
Spherical Waves	No	No	No	No	No	Yes
3D	No	No	No	Yes	Yes	Yes
MMWave	No	No	No	Yes	Partly	Yes
Dynamic Modeling	No	Very Limited	No	Limited	No	Yes

From the former table, we can see that WINNER 2, available in open source, has very detailed references and good level for ease use and is suitable for beginners to study, while QuaDRiGa as an extension of WINNER 2, may be a perfect choice for widened and advanced research accounting for 5G. The newest model, METIS, is not available in open source (only authorized use) and it has limited deliverable documents. In terms of the performance comparison, WINNER and IMT-Advanced models implemented versatile set environments, varying from indoor to outdoor and transitions. The COST 2100 model is closely similar to the WINNER models, while QuaDRiGa extends the WINNER models into a 3D model with geometric polarization and applies to terrestrial as well as satellite communications. In METIS, the model employed a combination of map-based and stochastic channel models, which is suitable for Massive MIMO. The model uses ray-tracing method to obtain large scale fading characteristic and 3GPP-like approaches to generate the small scale statistics. So far, QuaDRiGa fulfills all the features that allows to modeling in a promising way for 5G networks.

5. SIMULATION

5.1 Implementation and analysis of WINNER 2

As an elementary model, the focused was first on WINNER 2 channel. The Matlab-based open source model is provided at the WINNER official website [134]. The first step in the simulation was to set up a relevant fading channel, which can have single or multiple links. For the simplification, a system simulation with two mobile stations and one base station was implemented. The distances between mobile station and base station were 5 (1st mobile station) and 20 (2nd mobile station) meters, respectively. The field pattern for each elements is defined in WINNER Element Coordinate System (ECS), which actually is not suitable for complex simulation, but all array element are measured separately and the patterns are analytically descripted. In this case, the geometry are Uniform-Circular-Array (UCA) with 8, 2, and 4 elements, and radius of 20, 10, and 5 cm are defined to base station, 1st and 2nd mobile station respectively. The number of links were set to 2. A simple spectrum analysis is illustrated as Figure 5.1. The spectrum of the received signals at base station shows frequency selectivity, and the distance impact, where power is higher at close distance than at a longer distance mobile station between the transmitter and the mobile station.

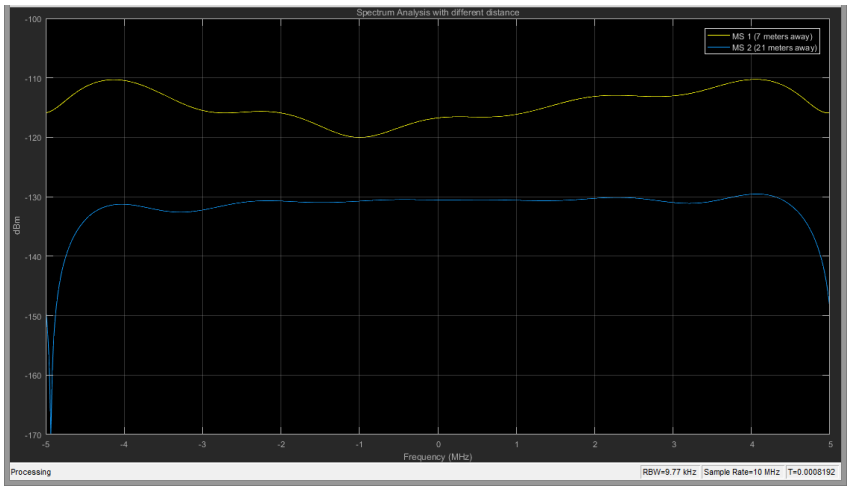

Figure 5.1 *Spectrum analyzer with different distance*

Furthermore, multiple base stations and mobile stations were implemented with multiple MIMO links. In the channel model, a base station with several sectors are assigned to mobile stations with an antenna array. First, 16 elements with a radius of 30 cm for base stations and 4 elements with radius of 5 cm for mobile stations are in UCA were defined. Totally, 6 links assigned with scenarios (B4, outdoor to indoor), (C2, urban macrocell outdoor to indoor), (C4, urban macrocell) [101] and NLOS propagation were mapped as shown in the Figure 5.2. The 1st base station is connected with the 1st (50m) and 2nd

(111.8m) mobile stations, the 2nd base station is connected to the 3rd (65m) mobile station. Meantime, the 3rd base station is connected to 4th (120.4m) and 5th (75m) mobile station.

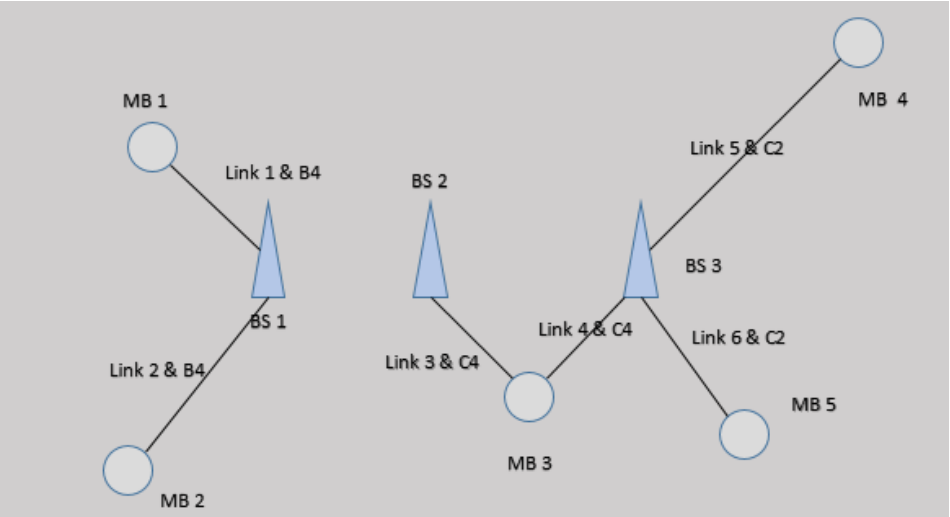

Figure 5.2 *Station layout*

The center frequency in this implementation is 5.25 GHz corresponding to WINNER 2 channel models. As results show in Figure 5.3, due to the same scenarios and almost the same distance, the CIR of 3rd and 4th links are similar but significantly worse than others. Meanwhile, the propagation in C2 scenario is measured with higher magnitude than the CIR in B4. It is the Author's view that, the propagation in link 6 with high power may be influenced less by shadow fading that the other links. Figure 5.4 illustrates the frequency sensitivity. The link connected to 4th mobile station has the largest average power, which is actually the same result as in the previous test. Practically, as assigning with the urban macro-cell outdoor-to-indoor scenario to the 4th and 5th mobile stations, and urban macro-cell scenario to the 3rd mobile station, the 5th link may propagate with more cluster and due to the reflection, the power received between 4th and 5th links are almost the same. The 6th link (with shortest transmitter-receiver distance) definitely has the largest power through the propagation.

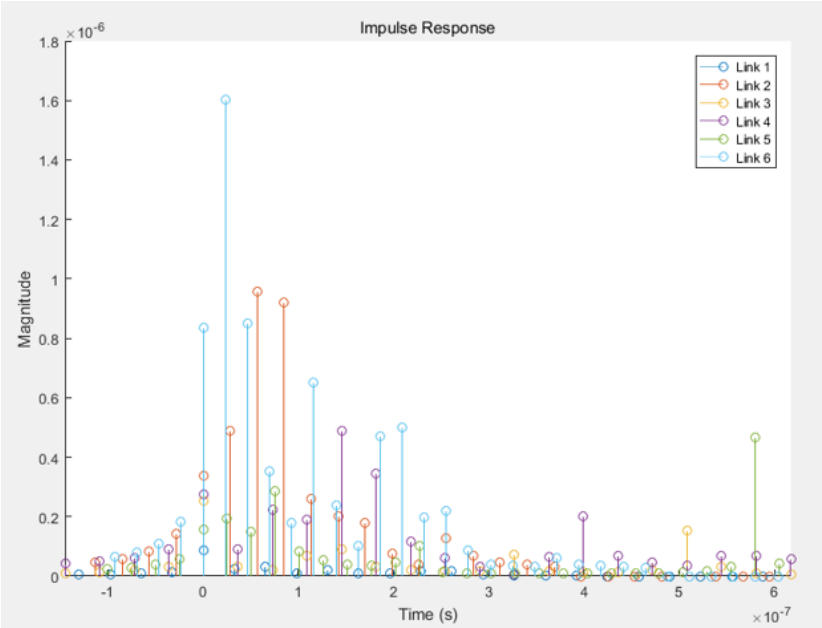

Figure 5.3 *Channel impulse response among different distance and scenarios*

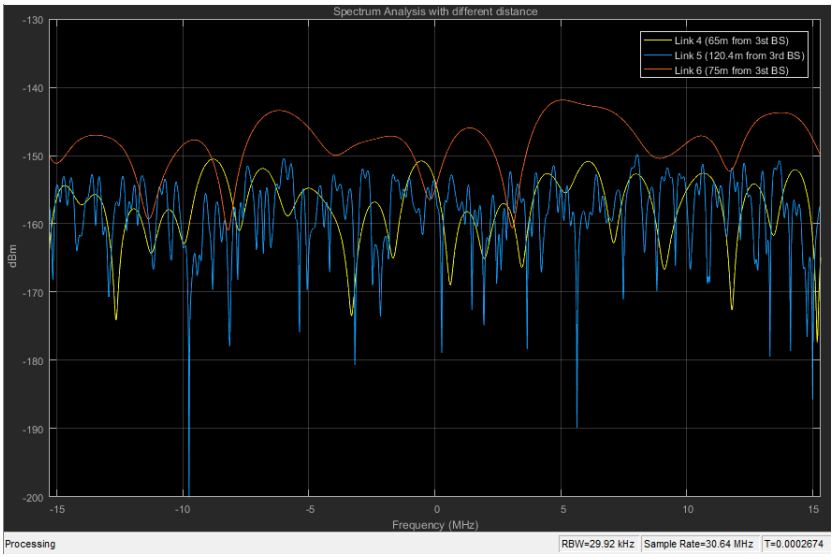

Figure 5.4 *Impulse response among three links*

Although WINNER channel model is constructed as antenna independent model, an antenna array model is necessary to obtain signals at the output of the radio-channel. This model is deterministic and permanent from the viewpoint of the simulation, and can be created independently from channel model simulations. Therefore certain type of array requires only single construction, which should be performed independently from WINNER 2 simulations - in pre-processing phase. It is not a good strategy to construct arrays each time when WINNER 2 models are used, instead defined antenna arrays should be stored and retrieved when needed. This becomes particularly important when large number of operations is performed in this phase, i.e. when 3D field patterns are rotated from ECS to ACS.

5.2 Comparison between WINNER 2 and QuaDRiGa

To implement the simulation work, all the original parameters are accordingly based on [134] and [36], as well as the propagation models such as path loss model and shadow model etc. Overall, the simulation work relative to WINNER 2 are based on [134], where the input user defined parameters, the MIMO radio link parameters and antenna parameters are described in [101]. The simulation of QuDRiGa is according to the [36].

In those two models, every path is split into 20 sub-paths with individually path delay. After extracting the channel coefficient and the delay corresponding to each sub-path, the channel impulse response was simulated, which illustrates the link performance. As seen in the Figure 5.5 (a), the power of multiple paths in WINNER 2 is distributed more intensively accounting for lower delay. On the contrary, the power at NLOS path around high delay is limited. In (b), both LOS and NLOS happens along with different delays, which is more uniform than in WINNER 2. In this case, WINNER 2 propagation environment is highly influenced by LOS path and QuDRiGa models are adapted to an extensive scenarios.

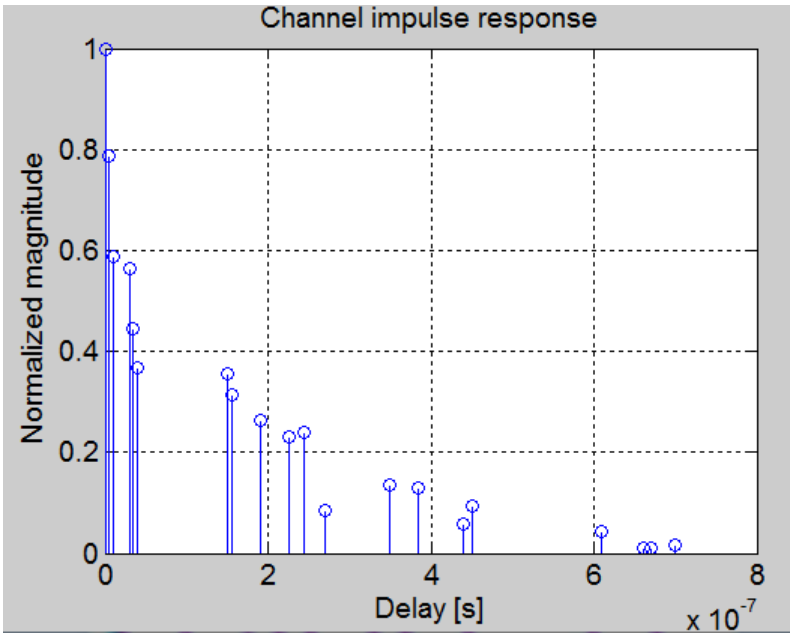

(a)

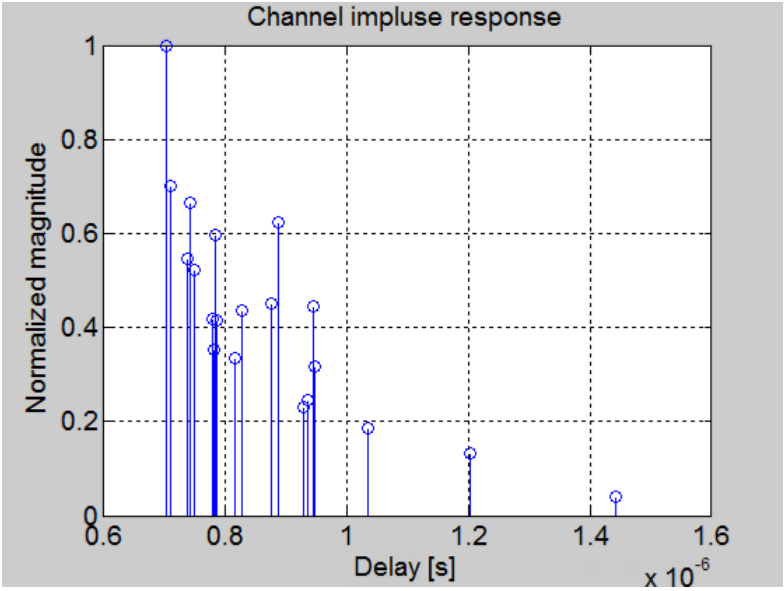

(b)

Figure 5.5 *Channel impulse* ***(a)*** *WINNER 2* ***(b)*** *QuDRiGa*

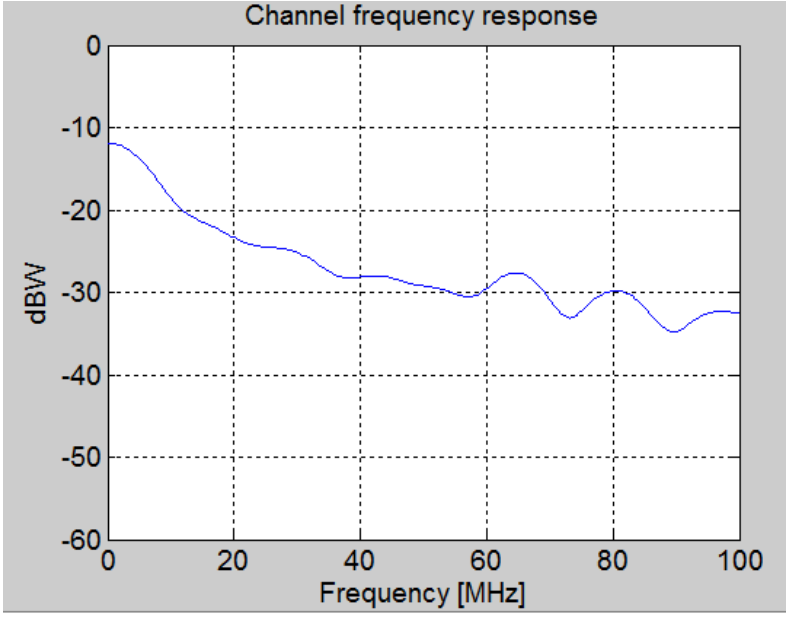

(a)

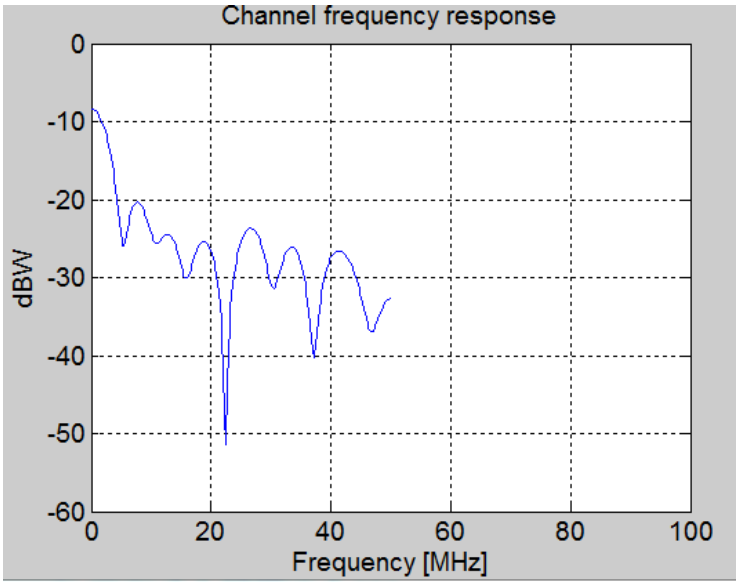

(b)

Figure 5.6 *Channel frequency response* ***(a)*** *WINNER 2* ***(b)*** *QuaDRiGa*

After a Discrete-time Fourier Transform (DTFT), with sample period of 0.0014s and 0,00056s in WINNER2, QuaDRiGa respectively, the corresponding frequency responses are obtained, as shown in Figure 5.6. Apparently, the channel frequency response of WINNER 2 is relatively flat compare to the result of QuDRiGa, where the amplitude of fluctuation of frequency response is larger and it is highly dependent to the frequency changes. Thus, in QuDRiGa, the propagation has a strong frequency selective fading due to the multiple path interference.

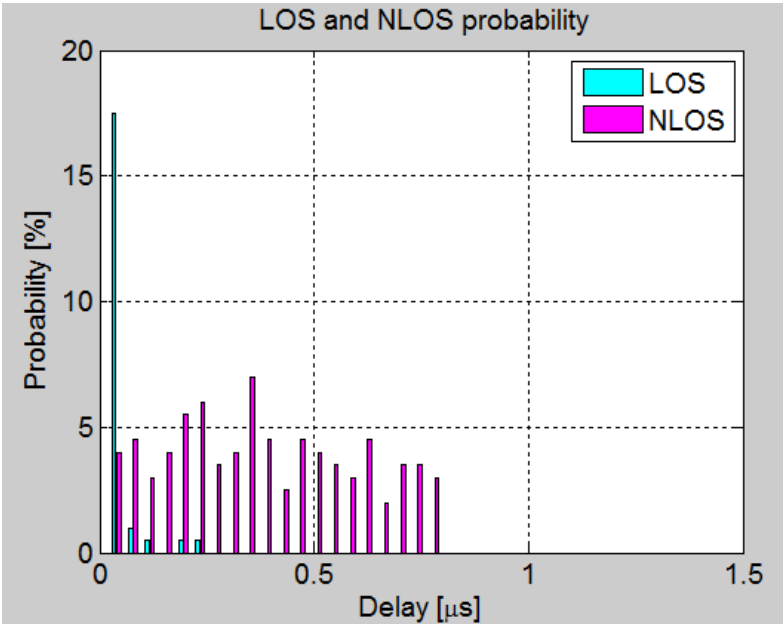

(a)

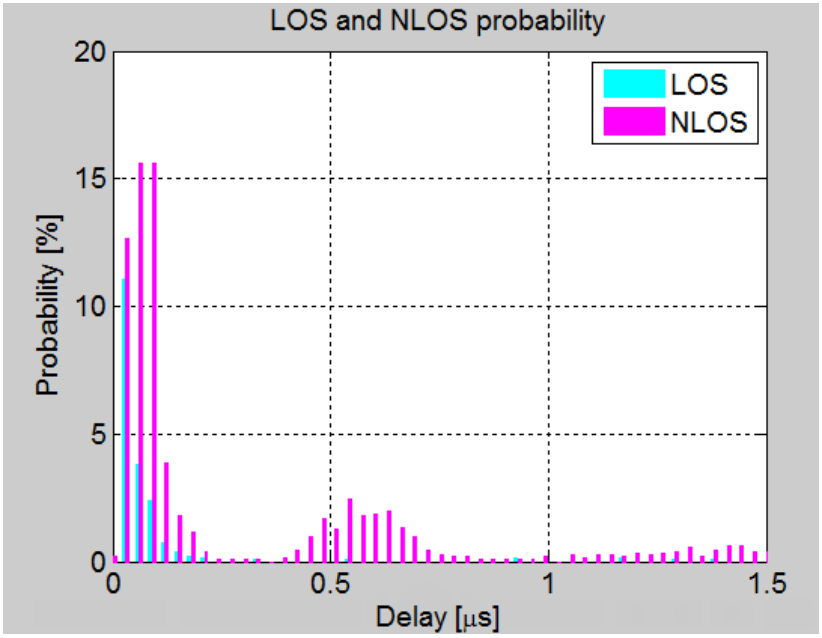

(b)

Figure 5.7 *LOS and NLOS probability* ***(a)*** *WINNER 2* ***(b)*** *QuaDRiGa*

The plot in Figure 5.7 shows the distribution of LOS and NLOS probability, where the channel coefficients together with the corresponding delays can be found in [36, 128]. Conclusively, the probability of a LOS path delay of WINNER 2 is larger than that of QuaDRiGa. Also the low path delays happen less in WINNER 2 NLOS propagation, than in QuaDRiGa. The probability of NLOS is comparatively large, even with low path delay. Thus, we can say that QuaDRiGa channel models are influenced by the NLOS path in a deeper way than WINNER 2.

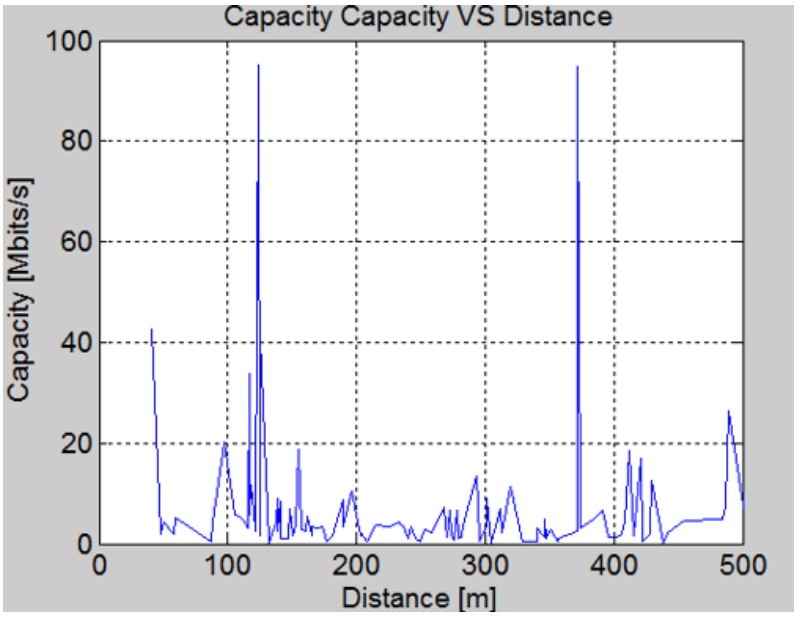

(a)

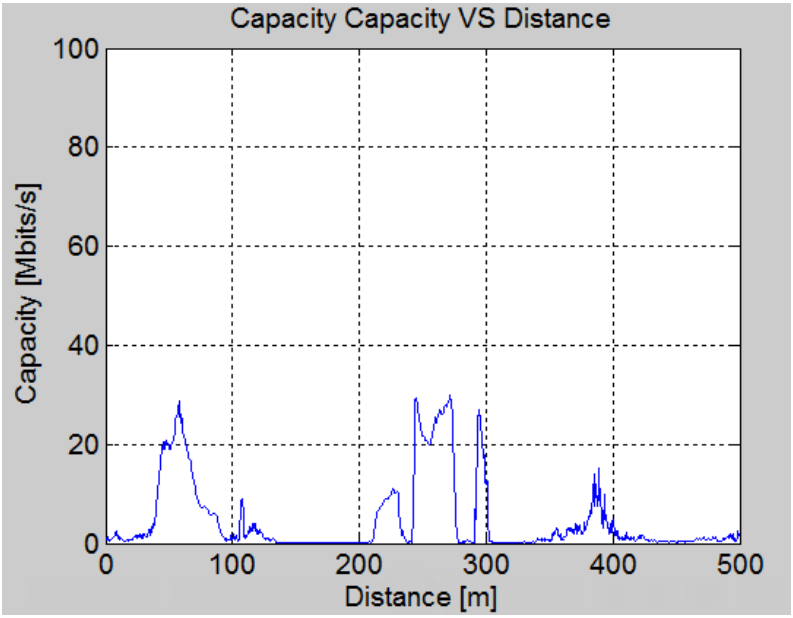

(b)

Figure 5.8 *Channel capacity versus distance* ***(a)*** *WINNER 2* ***(b)****QuaDRiGa*

From the simulation of Figure 5.8, we can know that both the WINNER 2 and QuaD-RiGa channel capacity are not responded to the distance. Because the channel capacity is not influenced directly by the distance, and no matter how the distance changes, both the LOS and NLOS paths are still existing. In this case, due to the frequency selective fading, the capacity of QuaDRiGa will remain almost the same. Moreover, WINNER 2 models are highly dependent on LOS propagation. Thus, the channel capacity of WIN-NER 2 shows dramatic peaks but in QuaDRiGa, it is just regular fluctuating. From other perspective, as illustrated in Figure 5.9, taking the probability at the 0.5 %, the observa-tion shows that WINNER 2 has a larger average capacity. Generally, WINNER 2 has a wider bandwidth and smaller fast fading than QuaDRiGa.

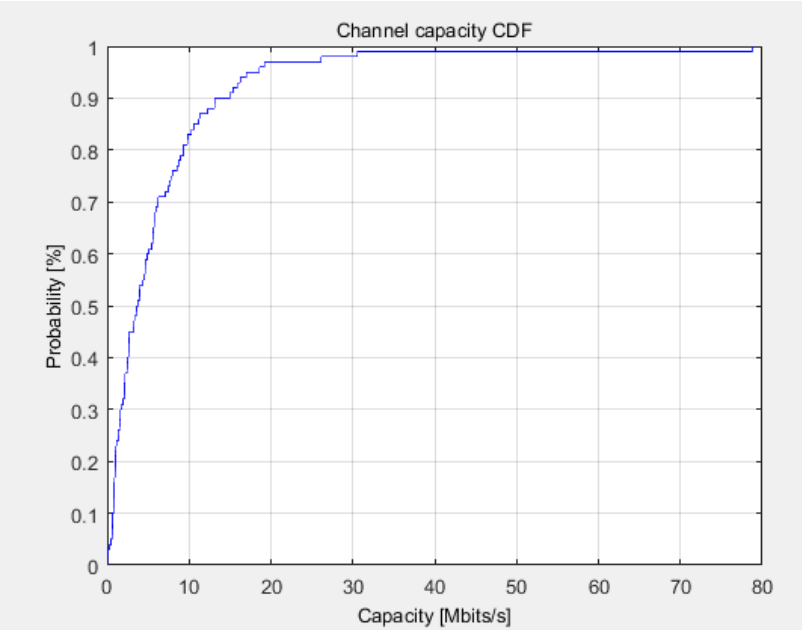

(a)

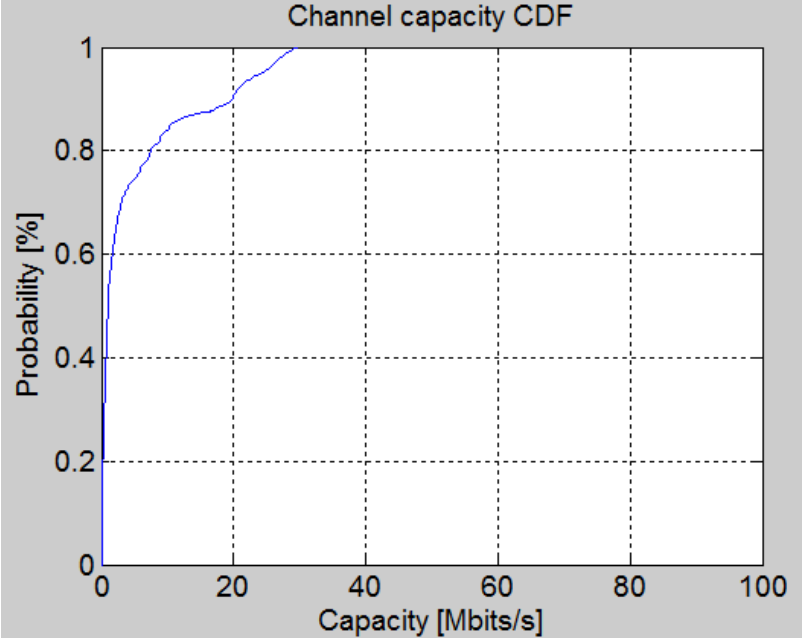

(b)

Figure 5.9 *Channel capacity* ***(a)*** *WINNER 2* ***(b)*** *QuaDRiGa*

6. CONCLUSIONS

5G networks aim to satisfy the extremely high traffic demand. At the same time, the mmWave provides abundant spectrum sources. Thus, a combination of 5G and mmWave will enable a high speed connected world serving a huge amount of users and devices. 5G mmWave channel modeling, as an efficient method to promote 5G and mmWave techniques maturity, needs to be accurate, applicable and sustainable. There are several existing mmWave channel models in the current literature. After reviewing them, we have focused on two main ones, available as open source: WINNER and QuaDRiGa. QuaDRiGa model is a statistical geometrical wideband channel mode, and it is extended from WINNER.

In this thesis, the performance of several mmWave channel models was compared according to literature overview and basic simulations. Firstly the CIR of two channel models was compared. The results showed that WINNER 2 channel model is much more relying on LOS signals, whereas the power of NLOS is much lower than in QuaDRiGa. In terms of the link performance, QuaDRiGa models with uniform distribution are adapted to a wider environment than WINNER 2. Moreover, the frequency response illustrates that QuaDRiGa model has a strong selective fading due to the multiple path interference. The simulation of LOS and NLOS distribution tells that the probability of LOS increases along with the small delay and large receiving power, while NLOS probability is more likely to be high with larger delay and weak power. Due to the strong LOS signals, WINNER 2 has a larger channel capacity than QuaDRiGa. It is clearly space for further research and verification. To conclude, a comparison table among mostly popular channel models was also included, including WINNER 2 and QuaDRiGa, which provide a direct view of channel performance.

REFERENCES

[1] Talukdar R, Saikia M. Evolution and Innovation in 5G Cellular Communication System and Beyond: A Study [J]. Computer Science, 2014.

[2] Elkashlan M, Duong T Q, Chen H H. Millimeter-wave communications for 5G: fundamentals: Part I [Guest Editorial] [J]. Communications Magazine IEEE, 2014, 52(9):52-54.

[3] Elkashlan M, Duong T Q, Chen H H. Millimeter-wave communications for 5G – Part 2: applications [Guest Editorial] [J]. IEEE Communications Magazine, 2015, 53(1):166-167.

[4] Boccardi F, Heath R W, Lozano A, et al. Five disruptive technology directions for 5G[J]. IEEE Communications Magazine, 2013, 52(2):74-80.

[5] High Rate 60 GHz PHY, MAC and HDMI PAL, ECMA Std. 387, Dec. 2008, ECMC TC48.

[6] Ajorloo H, Manzuri-Shalmani M T. Modeling Beacon Period Length of the UWB and 60-GHz mmWave WPANs Based on ECMA-368 and ECMA-387 Standards [J]. IEEE Transactions on Mobile Computing, 2013, 12(6):1201-1213.

[7] IEEE 802.15 WPAN Millimeter Wave Alternative PHY Task Group 3c (TG3c). [Online] Available: http://www.ieee802.org/15/pub/TG3c.html.

[8] Draft Standard for Information Technology-Telecommunications and Information Exchange Between Systems-Local and Metropolitan Area Networks-Specific Requirements-Part 11: Wireless LAN Medium Access Control (MAC) and Physical Layer (PHY) Specifications-Amendment 4: Enhancements for Very High Throughput in the 60 GHz Band, IEEE P802.11ad/ D9.0, Oct. 2012.

[9] Khan F, Pi Z. mmWave mobile broadband (MMB): Unleashing the 3–300GHz spectrum[C]// Sarnoff Symposium. IEEE, 2011:1-6.

[10] Pi Z, Khan F. An introduction to millimeter-wave mobile broadband systems [J]. IEEE Communications Magazine, 2011, 49(6):101-107.

[11] Pietraski, P., Britz, D., Roy, A, et al. Millimeter wave and terahertz communications: Feasibility and challenges. ZTE Communications, 2012, 10(4), 3–12.

[12] Rangan S, Rappaport T S, Erkip E. Millimeter-Wave Cellular Wireless Networks: Potentials and Challenges [J]. Proceedings of the IEEE, 2014, 102(3):366-385..

[13] Singh S, Mudumbai R, Madhow U. Interference Analysis for Highly Directional 60-GHz Mesh Networks: The Case for Rethinking Medium Access Control [J]. IEEE/ACM Transactions on Networking, 2011, 19(5):1513-1527.

[14] Chu H, Xu P, Jiang S, et al. Joint Design of Axis Alignment and Positioning for NLoS Indoor mmWave WLANs/WPANs[C]// IEEE, Vehicular Technology Conference. IEEE, 2014:1-6.

[15] Rappaport T S, Sun S, Mayzus R, et al. Millimeter Wave Mobile Communications for 5G Cellular: It Will Work! [J]. IEEE Access, 2013, 1(1):335-349.

[16] Roh W, Seol J Y, Park J, et al. Millimeter-wave beamforming as an enabling technology for 5G cellular communications: theoretical feasibility and prototype results [J]. IEEE Communications Magazine, 2014, 52(2):106-113.

[17] Roivainen A, Dias C F, Tervo N, et al. Geometry-Based Stochastic Channel Model for Two-Story Lobby Environment at 10 GHz [J]. IEEE Transactions on Antennas & Propagation, 2016, 64(9):3990-4003.

[18] Kim M, Takada J I, Chang Y, et al. Large scale characteristics of urban cellular wideband channels at 11 GHz [C]// European Conference on Antennas and Propagation. IEEE, 2015.

[19] Belbase K, Kim M, Takada J I. Study of propagation mechanisms and identification of scattering objects in indoor multipath channels at 11 GHz[C] // European Conference on Antennas and Propagation. IEEE, 2015:1-4.

[20] Daniels R C, Jr R W H. 60 GHz wireless communications: emerging requirements and design recommendations [J]. IEEE Vehicular Technology Magazine, 2007, 2(3):41-50.

[21] Smulders P F M. Statistical Characterization of 60-GHz Indoor Radio Channels [J]. IEEE Transactions on Antennas & Propagation, 2009, 57(10):2820-2829.

[22] Maccartney G R, Rappaport T S, Sun S, et al. Indoor Office Wideband Millimeter-Wave Propagation Measurements and Channel Models at 28 and 73 GHz for Ultra-Dense 5G Wireless Networks [J]. IEEE Access, 2015, 3:2388-2424.

[23] Rappaport T S, Maccartney G R, Samimi M K, et al. Wideband Millimeter-Wave Propagation Measurements and Channel Models for Future Wireless Communication System Design [J]. IEEE Transactions on Communications, 2015, 63(9):3029-3056.

[24] Hur S, Baek S, Kim B, et al. Proposal on Millimeter-Wave Channel Modeling for 5G Cellular System[J]. IEEE Journal of Selected Topics in Signal Processing, 2016, 10(3):454-469.

[25] Hur S, Cho Y J, Kim T, et al. Wideband spatial channel model in an urban cellular environments at 28 GHz[C] // European Conference on Antennas and Propagation. EurAAP, 2015.

[26] Azar Y, Wong G N, Wang K, et al. 28 GHz propagation measurements for outdoor cellular communications using steerable beam antennas in New York city[C]// IEEE International Conference on Communications. IEEE, 2013:5143-5147.

[27] Semkin V, Virk U, Karttunen A, et al. E-band propagation channel measurements in an urban street canyon[C]// European Conference on Antennas and Propagation. IEEE, 2015:1-4.

[28] Zhao X, Li S, Wang Q, et al. Channel Measurements, Modeling, Simulation and Validation at 32 GHz in Outdoor Microcells for 5G Radio Systems [J]. IEEE Access, 2017, 5(99):1062-1072.

[29] Rappaport T S, Heath R W, Daniels R C, et al. Millimeter wave wireless communications [M]. Prentice Hall, 2015.

[30] Vuokko Nurmela et al., “Initial channel models based on measurements”, D1.2, ICT-317669, METIS project, Apr. 2014. [Online]. Available: https://www.metis2020.com/wp-content/uploads/deliverbles/METIS_D1.2_v1.pdf

[31] MiWEBA, “D5.1: channel modeling and characterization,” FP7-ICT368721/D5.1, June 2014. [Online]. Available: http://www.miweba.eu/wp-content/uploads/2014/07/MiWEBA_D5.1_v1.011.pdf

[32] Samimi M K, Rappaport T S. Ultra-wideband statistical channel model for non line of sight millimeter-wave urban channels [C]// Global Communications Conference. IEEE, 2015.

[33] Thomas T A, Nguyen H C, Maccartney G R, et al. 3D mmWave Channel Model Proposal [C] // IEEE, Vehicular Technology Conference. IEEE, 2014:1-6.

[34] Li Q C, Wu G, Rappaport T S. Channel model for millimeter-wave communications based on geometry statistics[C]// GLOBECOM Workshops. IEEE, 2014:427-432.

[35] Study on Channel Model for Frequency Spectrum Above 6 GHz, TR 38.900, 3GPP. Sep. 2016. [Online]. Available: http://www.3gpp.org

[36] Jaeckel S, Raschkowski K, Borner K, et al. QuaDRiGa-Quasi Deterministic Radio Channel Generator, User Manual and Documentation, Fraunhofer Heinrich Hertz Institute, Tech. Rep. v1.4.8-571, 2016.

[37] IMT-2020 (5G) Promotion Group. 5G Vision and Requirements, white paper [EB/OL]. May. 2014. [Online]. Available: http://www.IMT-2020.cn

[38] Pi Z, Khan F. An introduction to millimeter-wave mobile broadband systems [J]. IEEE Communications Magazine, 2011, 49(6):101-107.

[39] Bleicher A. The 5G phones future. IEEE Spectrum, 2013, 50(7): 15-16.

[40] Ericsson White Paper. 5G Systems – enabling industry and society transformation. Jan. 201. [Online]. Available: https://www.ericsson.com/assets/local/news/2015/1/what-is-a-5g-system.pdf

[41] Huawei White Paper. 5G: A Technology Vision. Mar. 2014. [Online]. Available: http://www.huawei.com/en/publications/winwin-magazine/19/HW_329327

[42] 5G PPP Architecture Working Group. View on 5G Architecture. Version 1.0, July 2016. [Online]. Available: https://5g-ppp.eu/wp-content/uploads/2014/02/5G-PPP-5G-Architecture-WP-July-2016.pdf

[43] Marzetta T L. Noncooperative Cellular Wireless with Unlimited Numbers of Base Station Antennas [J]. IEEE Transactions on Wireless Communications, 2010, 9(11):3590-3600.

[44] Gao X, Edfors O, Rusek F, et al. Linear Pre-Coding Performance in Measured Very-Large MIMO Channels[C]// IEEE Vehicular Technology Conference, Vtc Fall 2011, 5-8 September 2011, San Francisco, Ca, Usa. DBLP, 2011:1-5.

[45] Marzetta T L, Caire G, Debbah M, et al. Special issue on massive MIMO. Journal of Communications and Networks, 2013, 15(4): 333-337.

[46] Ngo H Q, Marzetta T L, Larsson E G. Analysis of the pilot contamination effect in very large multicell multiuser MIMO systems for physical channel models. Proceedings of IEEE International Conference on Acoustics, Speech and Signal Processing (ICASSP), Prague, Czech Republic, 2011: 3464-3467.

[47] Yin H, Gesbert D, Filippou M, et al. A coordinated approach to channel estimation in large-scale multiple-antenna systems. IEEE Journal on Selected Areas in Communications, 2013, 31(2): 264-273.

[48] Li Y, Nam Y H, Ng B L, et al. A non-asymptotic throughput for massive MIMO cellular uplink with pilot reuse. Proceedings of IEEE Global Communications Conference (Globecom), Ottawa, Canada, 2012: 4500-4505.

[49] Lu L, Li G Y, Swindlehurst A L, et al. An Overview of Massive MIMO: Benefits and Challenges [J]. IEEE Journal of Selected Topics in Signal Processing, 2014, 8(5):742-758.

[50] Kenworthy G R. Self-cancelling full-duplex RF communication system: US, US5691978 [P]. 1997.

[51] Choiy J I, Jainy M, Srinivasany K, et al. Achieving single channel, full duplex wireless communication. In: Proceedings of ACM Annual International Conference on Mobile Computing and Networking, Chicago, 2010. 1–12

[52] Yu C H, Doppler K, Riberiro C B, et al. Resource Sharing Optimization for Device-to-Device Communications, 2011, 10(8):2752-2763.

[53] Wei L, Hu R, Qian Y, et al. Key elements to enable millimeter wave communications for 5G wireless systems [J]. IEEE Wireless Communications, 2014, 21(6):136-143.

[54] Faruque S. Free Space Propagation [M]// Radio Frequency Propagation Made Easy. Springer International Publishing, 2015:19-26

[55] Tian Z Y, Studio H. A Brief Discussion of 5G Key Technologies [J]. Mobile Communications, 2015.

[56] Richard M. Anite Leads 5G Radio Channel Model Development [J]. Microwave Journal, 2013, 56(12): 43-44.

[57] Wang C X, Haider F, Cao X Q, et al. Cellular architecture and key technologies for 5G wireless communication networks [J]. IEEE Communications Magazine, 2014, 52(2): 122-130

[58] You Xiaohu, Pan Zhiwen, Gao Xiqi, et al. The 5G mobile communications: the development trends and its emerging key techniques [J]. Science China Press, 2014, 44(5): 551-563.

[59] Hwang I S, Song B Y, Soliman S S. A holistic view on hyper-dense heterogeneous and small cell networks [J]. IEEE Communications Magazine, 2013, 51(6): 20-27

[60] Baldemair R, Dahlman E, Parkvall S, et al. Future wireless communications [C]// Vehicular Technology Conference. Dresden: IEEE, 2013: 1-5

[61] Liu S, Wu J, Koh C H, et al. A 25 Gb/s (/km 2) urban wireless network beyond IMT-advanced [J]. IEEE Communications Magazine, 2011, 49(2):122-129.

[62] Zhao Guofeng, Chen Jing, Han Yuanbing, Xu Chuan. Prospective network techniques for 5G mobile communication: A survey [J]. Journal of Chongqing University of Posts and Telecommunications (Natural Science Edition), 2015, 27 (4): 441-452.

[63] Galiotto C, Marchetti N, Doyle L. Flexible spectrum sharing and interference coordination for low power nodes in heterogeneous networks [C]// Vehicular Technology Conference. Quebee City: IEEE, 2012: 1-5.

[64] Jo Minho, Maksymyuk T, Batista R L, et al. A survey of converging solutions for heterogeneous mobile networks [J]. IEEE Wireless Communications, 2015, 21(6) :54-62.

[65] Dhillon H S, Ganti R K, Baccelli F, et al. Modeling and analysis of K-tier downlink heterogeneous cellular networks [J]. IEEE J Sel Area Commun, 2012, 30(3): 550-560.

[66] Lopez P D, Guvenc I, Chu X L. Mobility enhancements for heterogeneous networks through interference coordination [C]// IEEE Wireless Communications and Networking Conference Workshops. Paris: IEEE, 2012: 69-74.

[67] Prasad A, Lunden P, Tirkkonen O, et al. Mobility state based flexible inter-frequency small cell discovery for heterogeneous networks [C]// Personal Indoor and Mobile Radio Communications. London United Kingdom: IEEE, 2013: 2057-2061.

[68] Fettweis G, Krondorf M, Bittner S. GFDM - Generalized Frequency Division Multiplexing [C]// Vehicular Technology Conference, 2009. Vtc Spring 2009. IEEE. IEEE, 2009:1-4.

[69] ITU Internet Report 2005: The Internet of Things [J]. 2005..

[70] Jia X, Feng Q, Fan T, et al. RFID technology and its applications in Internet of Things (IoT) [C] // International Conference on Consumer Electronics, Communications and Networks. IEEE, 2012:1282-1285.

[71] TR 45.820 v13.1.0, “Cellular system support for ultra low complexity and low throughput internet of things,” Nov. 2015. [Online]. Available: http://www.3gpp.org/ftp/Specs/archive/45_series/45.820/45820-d10.zip

[72] Ericsson and Nokia Networks, “Further LTE physical layer enhancements for MTC,” RP-141660, 3GPP TSG RAN Meeting #65, Sept. 2014. [Online]. Available: http://www.3gpp.org/ftp/tsg_ran/tsg_ran/TSGR_65/Docs/RP-141660.zip

[73] Wang Y P E, Lin X, Adhikary A, et al. A Primer on 3GPP Narrowband Internet of Things [J]. IEEE Communications Magazine, 2017, 55(3):117-123.

[74] Marcus M, Pattan B. Millimeter wave propagation; spectrum management implications [J]. Microwave Magazine IEEE, 2005, 6(2):54-62.

[75] IEEE 802.15 WPAN Millimeter Wave Alternative PHY Task Group 3c (TG3c). [Online]. Available: http://www.ieee802.org/15/pub/TG3c.html.

[76] Draft Standard for Information Technology-Telecommunications and Information Exchange Between Systems-Local and Metropolitan Area Networks-Specific Requirements-Part 11: Wireless LAN Medium Access Control (MAC) and Physical Layer (PHY) Specifications-Amendment 4: Enhancements for Very High Throughput in the 60 GHz Band, IEEE P802.11ad/ D9.0, Oct. 2012.

[77] Niu Y, Li Y, Jin D, et al. A survey of millimeter wave communications (mmWave) for 5G: opportunities and challenges [J]. Wireless Networks, 2015, 21(8):2657-2676.

[78] Wei L, Hu R, Qian Y, et al. Key elements to enable millimeter wave communications for 5G wireless systems [J]. IEEE Wireless Communications, 2014, 21(6):136-143.

[79] Gutierrez F, Agarwal S, Parrish K, et al. On-chip integrated antenna structures in CMOS for 60 GHz WPAN systems[J]. IEEE Journal on Selected Areas in Communications, 2009, 27(8):1367-1378.

[80] Wei L, Hu R Q, Qian Y, et al. Enable device-to-device communications underlaying cellular networks: challenges and research aspects [J]. IEEE Communications Magazine, 2014, 52(6):90-96.

[81] Hu R Q, Qian Y. Heterogeneous Cellular Networks [J]. 2013.

[82] Lee K, Lee J, Yi Y, et al. Mobile data offloading: how much can WiFi deliver? [C]// International Conference. ACM, 2010:26.

[83] Mehrpouyan H, Matthaiou M, Wang R, et al. Hybrid millimeter-wave systems: a novel paradigm for hetnets [J]. Communications Magazine IEEE, 2015, 53(1):216-221.

[84] Qiao J, Shen X S, Mark J W, et al. Enabling device-to-device communications in millimeter-wave 5G cellular networks [J]. IEEE Communications Magazine, 2015, 53(1):209-215.

[85] Chaloupka Z. Technology and Standardization Gaps for High Accuracy Positioning in 5g [J]. IEEE Communications Standards Magazine, 2017, 1(1):59-65.

[86] M Pozar D. Microwave Engineering, 3rd [J]. IEEE Potentials, 2005, 8(2):11-13.

[87] Anderson C R, Rappaport T S. In-building wideband partition loss measurements at 2.5 and 60 GHz [J]. IEEE Transactions on Wireless Communications, 2016, 3(3):922-928.

[88] Alejos A V, Sanchez M G, Cuinas I. Measurement and Analysis of Propagation Mechanisms at 40 GHz: Viability of Site Shielding Forced by Obstacles [J]. IEEE Transactions on Vehicular Technology, 2008, 57(6):3369-3380.

[89] Gao Z, Dai L, Mi D, et al. MmWave massive-MIMO-based wireless backhaul for the 5G ultra-dense network [J]. IEEE Wireless Communications, 2015, 22(5):13-21.

[90] Goldsmith A. Wireless Communications [J]. 2005, 4(5):25-55.

[91] Lu X, et al., Convolutional Modeling and Antenna De-Embedding for Wideband Spatial mmWave Channel Measurement [J]. IEEE Wireless Communications and Networking Conference (WCNC), San Francisco, CA, USA, 2017, pp. 1-6.

[92] Collonge S, Zaharia G, Zein G E. Influence of the human activity on wide-band characteristics of the 60 GHz indoor radio channel [J]. IEEE Transactions on Wireless Communications, 2005, 3(6):2396-2406.

[93] 3rd Generation Partnership Project, “Further Advancements for E-UTRA Physical Layer Aspects (Release 9),” Cedex, France, 3GPP TR 36.814, Mar. 2010

[94] Akdeniz M R, Liu Y, Samimi M K, et al. Millimeter Wave Channel Modeling and Cellular Capacity Evaluation [J]. IEEE Journal on Selected Areas in Communications, 2014, 32(6):1164-1179.

[95] Alejos A V, Sanchez M G, Cuinas I. Measurement and Analysis of Propagation Mechanisms at 40 GHz: Viability of Site Shielding Forced by Obstacles [J]. IEEE Transactions on Vehicular Technology, 2008, 57(6):3369-3380.

[96] Li J. Rain Attenuation in Millimeter Wave Ranges [C]// International Symposium on Antennas, Propagation and Em Theory. 2006:1-4.

[97] Humpleman R J, Watson P A. Investigation of attenuation by rainfall at 60 GHz [J]. Proceedings of the Institution of Electrical Engineers, 1978, 125(2):85-91.

[98] Wang Y, Shi Z, Du M, et al. A millimeter wave spatial channel model with variant angles and variant path loss[C] // Wireless Communications and NETWORKING Conference. IEEE, 2016.

[99] 3GPP TR 36.873, "Study on 3D channel model for LTE," Tech. Rep., 2015

[100] Kyosti P, Meinila J, et al.,"IST-4-027756 WINNER II D1.1.1 V 1.1: WINNER II interim channel models," Tech. Rep., 2006. [Online]. Available: http://www.ist-winner.org

[101] Kyösti P, et al., "WINNER II channel models," Eur. Commission, Tech. Rep. D1.1.2 V1.1, Sep. 2007. [Online]. Available: http://projects.celticinitiative.org/winner+/WINNER2-Deliverables/

[102] Spatial Channel Model for Multiple Input Multiple Output (MIMO) Simulations, document 3GPP TR 25.996 V12.0.0, Sep. 2014.

[103] Hans D. Schotten, Mikko A. Uusitalo, "Intermediate description of the spectrum needs and usage principles", D5.1, ICT-317669, METIS project, August 2013. [Online]. Available: https://www.metis2020.com/wp-content/uploads/deliverables/METIS_D5.1_v1.pdf

[104] Leszek Raschkowski et al., "METIS Channel Models", D1.4, ICT-317669, METIS project, Feb. 2015. [Online]. Available: https://www.metis2020.com/wp-content/uploads/METIS_D1.4_v3.pdf

[105] Porter M. Competitive Advantage of Nations [J]. Competitive Intelligence Review, 1990, 1(1):14-14.

[106] Mikael F, Bogdan T, "Scenarios, requirements and KPIs for 5G mobile and wireless system", D1.1, ICT-317669, METIS project, May. 2015. [Online] Available: https://www.metis2020.com/wp-content/uploads/deliverables/METIS_D1.1_v1.pdf

[107] Rusyn, T.L. A study of the "slack-string" knife-edge diffraction model[C]// European Conference on Antennas and Propagation. IEEE, 2009:291-295.

[108] Walfisch J, Bertoni H L. A theoretical model of UHF propagation in urban environments [J]. IEEE Transactions on Antennas & Propagation, 1988, 36(12):1788-1796.

[109] Liang G, Bertoni H L. A new approach to 3-D ray tracing for propagation prediction in cities [J]. IEEE Transactions on Antennas & Propagation, 1998, 46(6):853-863.

[110] Shafi M, Zhang M, Moustakas A L, et al. Polarized MIMO channels in 3-D: models, measurements and mutual information [J]. IEEE Journal on Selected Areas in Communications, 2006, 24(3):514-527.

[111] Czink N, Zemen T, Nuutinen J P, et al. A Time-Variant MIMO Channel Model Directly Parametrised from Measurements [J]. EURASIP Journal on Wireless Communications and Networking, 2009, 2009(1):687238.

[112] Saito K, Kitao K, Imai T, et al. The Modeling Method of Time-Correlated MIMO Channels Using the Particle Filter[C]// Vehicular Technology Conference. IEEE, 2011:1-5.

[113] Jaeckel S, Raschkowski L, Kai B, et al. QuaDRiGa: A 3-D Multi-Cell Channel Model With Time Evolution for Enabling Virtual Field Trials [J]. IEEE Transactions on Antennas & Propagation, 2014, 62(6):3242-3256.

[114] Pedersen K I, Mogensen P E, Fleury B H. Power azimuth spectrum in outdoor environments [J]. Electronics Letters, 1997, 33(18):1583-1584.

[115] Jaeckel S, Kai B, Thiele L, et al. A Geometric Polarization Rotation Model for the 3-D Spatial Channel Model [J]. IEEE Transactions on Antennas & Propagation, 2012, 60(12):5966-5977.

[116] Chong C C, Watanabe F, Inamura H, et al. Performance comparison of the 3GPP/3GPP2 SCM and ITU-R IMT-Advanced MIMO channel models[C]// IEEE, International Symposium on Personal, Indoor and Mobile Radio Communications. IEEE, 2010:890-894.

[117] Chen G, Liu S, Zhu W. Analysis of doppler power spectral for MIMO channel based on 3GPP-SCM [J]. Journal of Chongqing University of Posts & Telecommunications, 2015.

[118] Sui W W, Jing X R, Zhou W, et al. Simulation of channel model of smart antenna system based on 3GPP-SCM [J]. Journal of Chongqing University of Posts & Telecommunications, 2011.

[119] Meinilä J et al., “Determination of Propagation Scenarios,” Eur. Commission, Tech. Rep. D5.2, Jul 2004. [Online]. Available:http://projects.celtic-initiative.org/winner+/DeliverableDocuments/D5.2_v1.1.pdf

[120] Daniel S. Baum et al., “Final Report on Link Level and System Level Channel Models,” Eur. Commission, Tech. Rep. D5.4 V1.4, Nov. 2005. [Online]. Available: http://projects.celtic-initiative.org/winner+/DeliverableDocuments/D5.4.pdf

[121] Jorn von Hafen et al., “System Requirements,” Eur. Commission, Tech. Rep. D7.1, Jul 2004. [Online]. Available: http://projects.celtic-initiative.org/winner+/DeliverableDocuments/D7.1.pdf

[122] Poutanen J, Haneda K, Liu L, et al. Parameterization of the COST 2100 MIMO channel model in indoor scenarios[C]// European Conference on Antennas and Propagation. IEEE, 2011:3606-3610.

[123] Virk U T, Haneda K, Wagen J F. Dense multipath components add-on for COST 2100 channel model[C]// European Conference on Antennas and Propagation. IEEE, 2015:1-5.

[124] Andrés Navarro C, Carlos A. Ardila, Duván Javier Mejía. Some comparison between propagation models in Cost 2100 Cali Reference Scenario [J]. 2009, 7(13).

[125] Eastwood L, Migaldi S, Xie Q, et al. Mobility using IEEE 802.21 in a heterogeneous IEEE 802.16/802.11-based, IMT-advanced (4G) network[J]. IEEE Wireless Communications, 2008, 15(2):26-34.

[126] Loa K, Wu C C, Sheu S T, et al. IMT-advanced relay standards [WiMAX/LTE Update] [J]. IEEE Communications Magazine, 2010, 48(8):40-48.

[127] Parkvall S, Furuskar A, Dahlman E. Evolution of LTE toward IMT-advanced [J]. IEEE Communications Magazine, 2011, 49(2):84-91.

[128] Gubbi J, Buyya R, Marusic S, et al. Internet of Things (IoT): A vision, architectural elements, and future directions [J]. Future Generation Computer Systems, 2012, 29(7):1645-1660.

[129] Mumford R. IMT-2020 Makes Progress in Developing 5G Standard [J]. Microwave Journal, 2016.

[130] Blanchard N. How ITU, 5GPPP, NGMN and others will create the standard for 5G [J]. Fiercewirelesstech, 2015.

[131] Waldhauser D S, Baltar L G, Nossek J A. Comparison of Filter Bank Based Multicarrier Systems with OFDM[C]// APCCAS 2006 - 2006 IEEE Asia Pacific Conference on Circuits and Systems. IEEE, 2006:976-979.

[132] Vakilian V, Wild T, Schaich F, et al. Universal-filtered multi-carrier technique for wireless systems beyond LTE[C]// GLOBECOM Workshops. IEEE, 2014:223-228.

[133] Berg J E. A recursive method for street microcell path loss calculations[C]// IEEE International Symposium on Personal, Indoor and Mobile Radio Communications, 1995. Pimrc'95. Wireless: Merging Onto the Information Superhighway. IEEE, 1995:140-143 vol.1.

[134] Milan Narandžić et al., “IST-4-027756 Matlab SW documentation of WIM2 model,” Tech. Rep., 2007 [Online]. Available: http://www.ist-winner.org